ASTRONOMICAL INSTITUTE
SLOVAK ACADEMY OF SCIENCES

CONTRIBUTIONS OF THE ASTRONOMICAL OBSERVATORY SKALNATÉ PLESO

• VOLUME XLIX •

Number 3

December 2019

ISSN: 1336–0337 (on-line version)

CODEN: CAOPF8

Editorial Office: Astronomical Institute of the Slovak Academy of Sciences
SK - 059 60 Tatranská Lomnica, The Slovak Republic

CONTENTS

STARS

ERASMUS+/OPTICON school: Observational astrophysics: from proposals to publication

The Contributions of the Astronomical Observatory Skalnaté Pleso
are available in a full version
in the frame of ADS Abstract Service
and can be downloaded in a usual way from the URL address:

http://adsabs.harvard.edu/

as well as from the web-site of
the Astronomical Institute of the Slovak Academy of Sciences
on the URL address:

https://www.astro.sk/caosp/

The journal is covered/indexed by:

Thomson Reuters services (ISI)
Science Citation Index Expanded (also known as SciSearch®)
Journal Citation Reports/Science Edition

SCOPUS

Contrib. Astron. Obs. Skalnaté Pleso **49**, 493 – 502, (2019)

Diffuse ionizing radiation in nebular envelopes of symbiotic novae V1016 Cyg and HM Sge

M. Skulskyy[1], B. Melekh[2] and O. Buhajenko[2]

[1] *Department of Physics, Lviv Polytechnic National University, 79013, Lviv, Ukraine, (E-mail: mysky@polynet.lviv.ua)*

[2] *Department of Astrophysics, Ivan Franko National University of Lviv, 79005, Lviv, Ukraine, (E-mail: bohdan.melekh@lnu.edu.ua)*

Received: May 13, 2019; Accepted: June 26, 2019

Abstract. The ionizing structure of the nebular envelopes of the symbiotic novae V1016 Cyg and HM Sge were determined using Ferland's photoionization code *Cloudy* upgraded by our method *DiffRaY* for a detailed calculation of the diffuse ionzing radiation. Our calculations are based on the optimal photoionization models, obtained previously for these objects using the standard code *Cloudy* that takes into account the diffuse ionizing radiation using an *outward only approximation*. In the present paper we compare the results of the photoionization modelling of V1016 Cyg and HM Sge nebular envelopes performed using both detailed and *outward only* methods. It was shown that the approximate fast *outward only* method can be used for the modelling of these objects.

Key words: symbiotic — novae — photoionization modelling
PACS number(s): 97.80.Gm, 98.38.Ly, 98.38.-j, 52.70.-m, 95.75.Pq, 07.05.Tp

1. Introduction

Most researchers (see, for example, Sanad (2017); Arkhipova et al. (2015); Parimucha et al. (2001); Eyres & Bode (2001); Rudy et al. (1990); Schmid & Schild (1990); Muerset et al. (1991); Muerset & Nussbaumer (1994)) are adopting the following model of the symbiotic novae: a hot white dwarf (WD) and cold red giant that lost its matter due to the stellar wind and accretion of the matter onto the hot component. Most probably, both V1016 Cyg and HM Sge contain an evolved cool giant of the Mira type and a WD accreting from the giant's wind. They are classified as symbiotic novae because they showed one nova-like eruption in the past. In the present work we investigate the nebular envelopes of the symbiotic novae V1016 Cyg and HM Sge using photoionization modelling (PhM) methods. The spherical symmetry for the nebular envelope with the white dwarf in its center was adopted. The real shape of these objects can deviate from the spherical one, but at present details of such deviations are unknown with required precision due to a compact envelope size relatively to the observer. The binary system is also non-spherical, but we suggest that this is not important for modelling because the size of the binary system is

significantly smaller than the one of nebular envelope. This nebular envelope consist of matter ejected during nova explosion(s). Of course, it can also be mixed with the wind material from the cool red giant. It must be noted that in our models the nebular envelope has an inner radius. It means that between the binary system and the nebula matter is absent. Thus, under such assumptions, the above mentioned mixing of the wind material with envelope is possible only during a nova explosion. In such binary system the role of main ionizing source for the nebular envelope belongs to the hot star and, maybe, to the accretion disk. The calculation of models stops at the ionization front (where T_e drops below 4000K), because emission lines arise within an ionized part of the nebula (the calculated intensities of these lines are used to compare with the corresponding observed data).

Emission line spectra of these symbiotic novae are similar to the ones for planetary nebulae envelopes. It allowed us to perform the photoionization modelling of these objects in our previous paper (Holovatyi et al., 2019) using the semi-empirical density distribution law obtained by Golovatyi & Malkov (1992) from analysis of the isophote maps of planetary nebulae. The radial ditribution of the gas density was approximated by equation (6) from Golovatyi & Malkov (1992). If we put optimal values (7) from the above paper to this approximating equation, we obtain the following expression for description of the radial density distribution within the nebula:

$$n_H(r) \;=\; \frac{x^2\left(1+3e^{-1.2x}\right)}{\left(x^2-1\right)^2+0.36r_c^{-0.43}x^2}DP, \qquad (1)$$

where r is the distance from the center of the nebula (and from the ionizing source) to the modelling layer of the nebula, $x = r/r_c$, r_c is the characteristic radius that is close to the position of maximum of the radial hydrogen density distribution, the so-called density parameter $DP \equiv A/r_c^2$, and A is a parameter characterizing the mass-loss rate by the star into the stellar wind. If we assume $r = r_c$ in expression (1), then we obtain the expression for $n_H(r_c)$ determination as a function of parameters DP and r_c. Because the values of $n_H(r_c)$ and DP were determined during a search of optimal models of V1016 Cyg and HM Sge in the paper by Holovatyi et al. (2019), the value of r_c can be directly determined from this expression.

In Holovatyi et al. (2019) we have demostrated the similarity of the diagnostic electron density distribution in these objects over ionization potentials of the corresponding ions, emitting in the corresponding ionization zones, to the the radial distribution defined by the above mentioned semi-empirical density distribution law. Therefore, in Holovatyi et al. (2019) we performed the photoionization modelling using the density distribution representation from Golovatyi & Malkov (1992).

In Holovatyi et al. (2019) we used our three stages method (Melekh et al., 2015) based on Ferland's photoionization code *Cloudy v08.00* (Ferland,

2008) to search for the optimal photoionization models for nebular envelopes of V1016 Cyg and HM Sge. The optimal models were found using the so-called *outward only* approximation that is also a default method for calculation of diffuse ionizing radiative transfer in the code *Cloudy* (Ferland, 2008). The *outward only* method is fast and, thus, very good for the search of the optimal photoionization models (such a search requires the calculation of thousands of photoionization models). But in Buhajenko & Melekh (2018) we showed that in the case of the inhomogenious distribution of matter the usage of the *outward only* approximation sometimes can be incorrect, because it causes (*sometimes*) incorrect reproducing by the model of the emission lines in the outer part of the nebular envelope. Therefore it is necessary to be sure that our optimal models, obtained in paper Holovatyi et al. (2019), are correct. To solve this task, in the present paper we recalculated the photoionization models for V1016 Cyg and HM Sge with values of input parameters obtained as a result of optimizing PhM in Holovatyi et al. (2019) using a detailed method (Buhajenko & Melekh, 2016) for calculation of the diffuse ionizing radiative transfer. For this purpose we used the code *Cloudy* (Ferland, 2008) upgraded by our method (Buhajenko & Melekh, 2016) for calculation of the diffuse ionizing radiation in a detailed way. Then we compare resulting models with the ones obtained previously by Holovatyi et al. (2019) using the *outward only* approximation.

2. Detailed method for calculation of diffuse ionizing radiative transfer

For a precise PhM calculation of diffuze ionizing radiation, the so-called *Detailed method* should be used. In this method equations for diffuze ionizing radiative transfer should be solved across all directions with the subsequent integration over all directions (see details in Buhajenko & Melekh (2016, 2018)). However, the usage of such approach to ionization-recombination, energetic and statistical equilibrum equations is very time-consuming even for modern powerful computer clusters. To avoid this problem the approximate methods (*outward only* or *on the spot*, see details in Ferland, 2008) for a diffuse ionizing radiative transfer calculation are usually used. To accelerate the *Detailed method* in Buhajenko & Melekh (2016, 2018) we have proposed to use gradual decreasing of an integration step until the required precision be achieved. Also, the procedure for a diffuse ionizing radiative transfer calculation in our approach is developed as a separate code *DiffRaY* [1] that does not require any implementation in the photoionization code. It just needs the emission line and continuum emissivities spatial map of diffuse radiation calculated by the photoionization code at the first global iteration step (over all modelling volume) as well as an opacity map. The initial emissivities map of diffuse ionizing radiation can be calculated using

[1]The code DiffRaY and its description can be downloaded from http://old.physics.lnu.edu.ua/depts/KAF/DiffRay/

one of the above mentioned approximate methods, or it can be simply neglected (to adopt zero values for diffuse emissivities). As in Holovatyi et al. (2019) for PhM we used Ferland's code code *Cloudy* (Ferland, 2008).

Table 1. The input parameters of photoionization models obtained in Holovatyi et al. (2019) as a result of the optimimal photoionization model search for nebular envelopes of V1016 Cyg and HM Sge.

Input parameters	V1016 Cyg	HM Sge
D [pc]	1521	1273
log L_*[erg/s]	37.50	38.13
log $T_{ef}[K]$	5.128	5.087
log $n_H(r_c)[\mathrm{cm}^{-3}]$	6.502	6.607
log(DP)	7.210	7.333
log r_{in} [cm]	14.41	14.93
log He/H	-1.095	-0.963
log N/H	-4.107	-3.776
log O/H	-4.035	-3.524
log Ne/H	-4.748	-4.197
log S/H	-5.153	-4.290
log Ar/H	-6.061	-5.292
$Dust\ factor$	0.438	1.290

In Table 1 the values of input parameters of photoionization models obtained in Holovatyi et al. (2019) as a result of the optimimal photoionization model search for nebular envelopes of V1016 Cyg and HM Sge are given. These parameters characterize the distance D from the Earth to the objects, the energy distribution in the spectrum of the central star that is the main source of the ionizing radiation (luminosity L and effective temperature T_{ef}), the hydrogen density $n_H(r_c)$ at the characteristic radius r_c, the density parameter DP (see above the description of Eq. 1), the internal radius r_{in} of the nebular envelope, the relative abundances of chemical elements, and the $Dustfactor$ for dust grains abundance adopted by default in the code *Cloudy*.

As in Holovatyi et al. (2019) all models were calculated in spherical symmetry and their calculations were stopping at the ionization front (where T_e drops below 4000K). We used these data for PhM of these objects based on the *Detailed method* for calculation of diffuse ionizing radiative transfer. For our purpose in the present work the global iterations convergence accuracy of 2% was adopted during a detailed calculation of diffuse ionizing radiative transfer using code *DiffRaY*. Covergence was achived after the third global iteration for both models of the the above objects. Also, it must be noticed that values of distances in Table 1 are smaller than those given in Muerset et al. (1991); Muerset & Nussbaumer

(1994). In these papers the distances to V1016 Cyg and HM Sge were determined using a period-luminosity (PL) relation that is used in the cases where a Mira is present in a symbiotic system. We determined the distances using optimized photoionization modelling (OPhM) method (see description of the method in (Melekh et al., 2015)). During OPhM the distance is a free parameter, and main observed parameters that are responsible for determination of its value are the angular size of the ionized nebular envelope and the observed flux in Hβ emission line. We suppose that for such peculiar objects as V1016Cyg and HM Sge the difference in results obtained by OPhM- and PL-methods should be considered in future investigations. The aim of the present paper did not include this task.

3. Results, analysis and conclusions

In Figs. 1 and 2 the radial distibutions of the electron temperature and density as well as [O III] 5007Å and [O III] 4363Å lines emissivity, obtained during PhM of nebular envelopes of V1016 Cyg and HM Sge using the *Outward Only* approximation as well as the *Detailed method*, are shown. Also in these figures there are shown zoom-ins of the nebular region containing the ionization front where the differences caused by the usage of different methods for calculation of diffuse ionizing radiative transfer, are maximal. As it was expected, the volume of the ionized nebular environment in the case of the *Detailed method* usage is a little bit smaller, because in this case the ionizing radiation is propagating in all directions, not in the outward only one as in the corresponding approximate method. The similar results were obtained in our previous works Buhajenko & Melekh (2016, 2018) for planetary nebulae envelopes and HII regions.

As it was mentioned above, in our models the nebular envelope has the inner radius r_{in} (between the binary system and the nebula the matter is absent). Eq. (1) was obtained by Golovatyi & Malkov (1992) on the basis of analysis of isophote maps of 10 real nebular objects under the assumption of their spherical symmetry. This equation has the maximum and the density decreases relatively to it in both directions (outward and inward). Such a radial hydrogen density distribution causes a similar distribution of the electron density N_e. The deviations of N_e from the hydrogen density distribution can be caused only by the presence of heavy elements in the nebula, which are the additional sources of electrons during photoionization. It can be seen that the character of the N_e radial distribution in the case of HM Sge differs from the one for V1016 Cyg. While in the case of the V1016 Cyg optimal model we see that this distribution is very similar to the one for $n_H(r)$ defined by expression (1), the maximum of the N_e distribution in the optimal model for HM Sge is very close to the inner radius r_{in} of the nebular envelope. This result was obtained because r_{in} was a free parameter during OPhM and it can reach the values larger than r_c. We suggest that such 'freedom' for variation of r_{in} is good, because it allows us to change slightly the character of the radial density distribution in the nebula

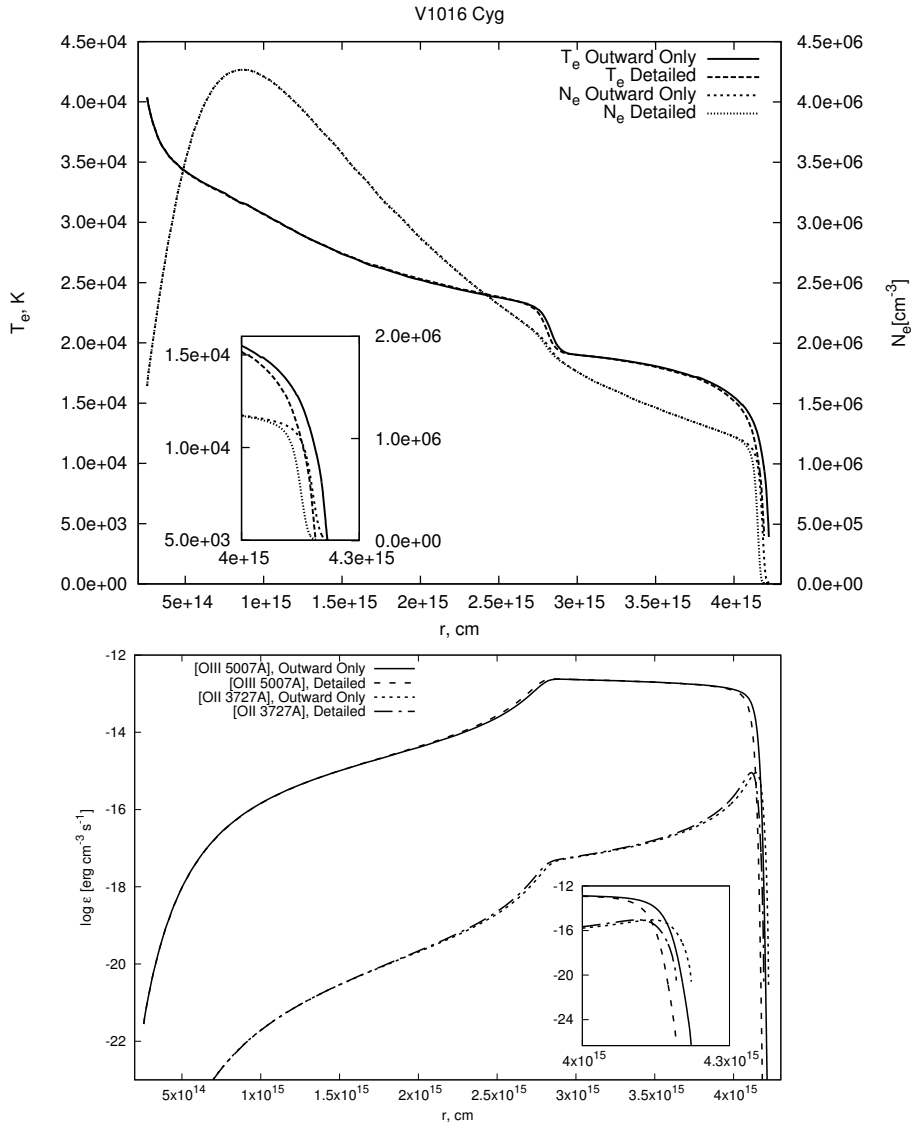

Figure 1. Comparison of the radial distributions of the electron temperature T_e and density N_e (top) as well as emissivities ϵ in [O III] and [O II] emission lines (bottom) obtained by our PhM of the V1016 Cyg nebular envelope using the *Outward only* approximation and the *Detailed* method for calculation of diffuse radiation field. Results are very similar (see the text for details).

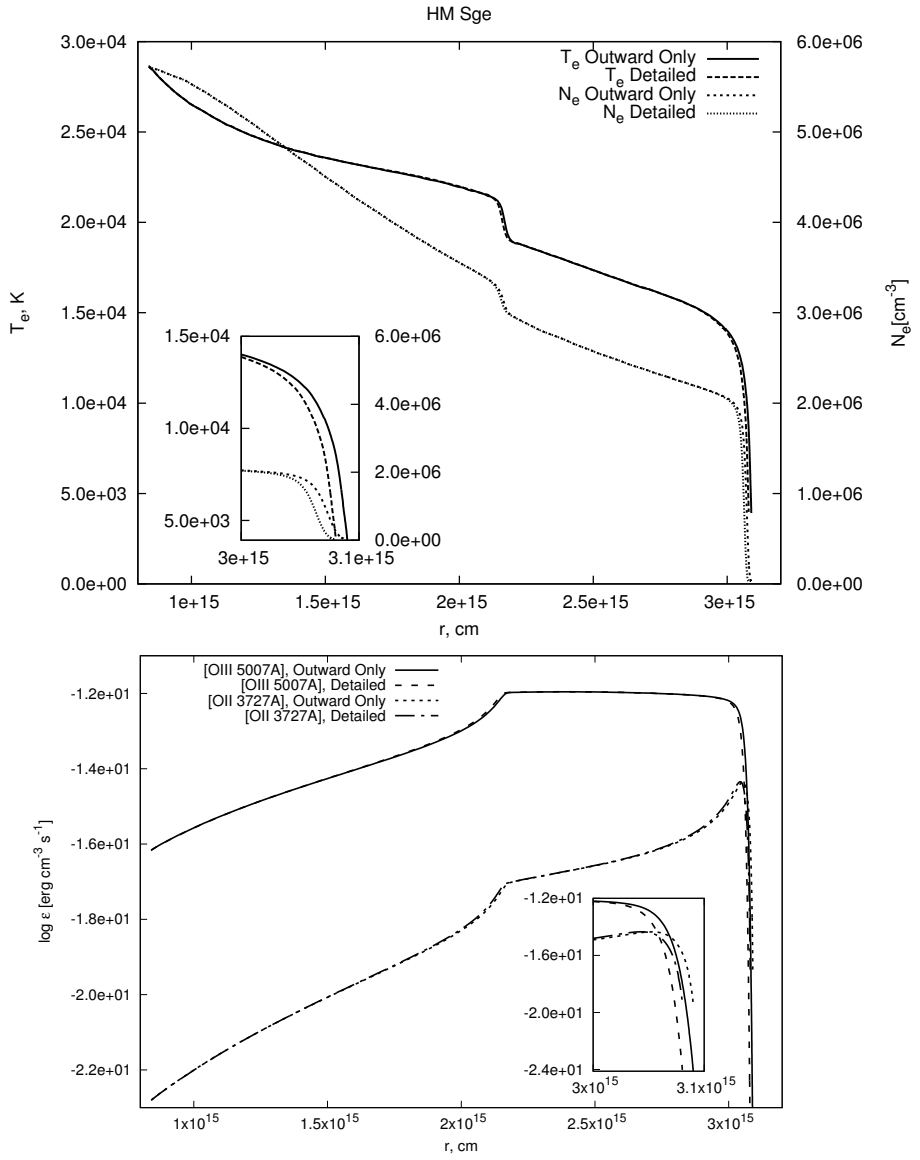

Figure 2. Comparison of radial distributions of the electron temperature T_e and density N_e (top) as well as emissivities ϵ in [O III] and [O II] emission lines (bottom) obtained by our PhM of the HM Sge nebular envelope using the *Outward only* approximation and the *Detailed* method for calculation of diffuse radiation field. Results are very similar (see the text for details).

Table 2. Comparison of the synthetic emission line spectra of nebular envelopes of V1016 Cyg and HM Sge obtained in Holovatyi et al. (2019) as a result of the search of the optimal photoionization model using the approximate *Outward Only* method, with results of PhM with the same optimal input parameters but using the *Detailed method* for calculation of diffuse ionizing radiative transfer. Deviations of these values obtained using the *Outward Only* approximation from the ones calculated using the *Detailed method* were determined using absolute values of parameters (not in a logarithmic scale).

Model of object:	V1016Cyg			HMSge		
Parameter	Outward Only	Detailed method	Δ^*, %	Outward Only	Detailed method	Δ^*, %
$\log L(\mathrm{H}\beta)$	30.546	30.543	-0.7	30.910	30.907	-0.7
[O II]λ3727/H$_\beta$	0.001	0.001	0.0	0.002	0.002	0.0
[O III]λ5007/H$_\beta$	1.791	1.791	0.0	3.791	3.807	0.4
[O III]λ4959/H$_\beta$	0.593	0.593	0.0	1.254	1.259	-0.3
[O III] λ4363/H$_\beta$	0.283	0.285	1.1	0.766	0.775	-0.5
He I λ4471/H$_\beta$	0.023	0.023	0.0	0.034	0.034	0.0
He I λ5876/H$_\beta$	0.088	0.089	0.0	0.134	0.135	0.0
He II λ4686/H$_\beta$	0.420	0.428	1.9	0.559	0.557	-0.4
[N II] λ6548/H$_\beta$	0.008	0.008	0.0	0.009	0.009	0.0
[N II] λ6584/H$_\beta$	0.022	0.022	0.0	0.025	0.025	0.0
[N II] λ5755/H$_\beta$	0.022	0.022	0.0	0.038	0.038	0.0
[S III]λ9532/H$_\beta$	0.131	0.130	-0.8	0.038	0.038	0.0
[S III]λ9069/H$_\beta$	0.052	0.052	0.0	0.583	0.580	-0.5
[S II] λ6716/H$_\beta$	-	-	-	0.001	0.001	0.0
[S II] λ6731/H$_\beta$	-	-	-	0.003	0.003	0.0
[S II] λ4070/H$_\beta$	0.021	0.021	0.0	0.117	0.116	-0.9
[S II] λ4078/H$_\beta$	0.006	0.006	0.0	0.029	0.029	0.0

* $\Delta = (OutwardOnly - DetailedMethod)/DetailedMethod$

during a search for the optimal photoionization model. The maximum within the radial density distribution can be caused by the shock wave that has created during a nova explosion. We think that obtained from our photoionization modelling the radial density distributions of matter contain the information that can be useful in future hydrodynamical simulations of V1016 Cyg and HM Sge evolution, which will allows us to explain the differences between their nebular characteristics.

It must be noted that a jump (or rapid decreasing) of T_e and N_e values within radii of $(2.7 - 2.9) \times 10^{15}$cm in models of V1016 Cyg and $(2.1 - 2.2) \times 10^{15}$cm in the ones of HM Sge are still present in results obtained using the *Detailed method*. As it was shown in Holovatyi et al. (2019) this jump separates the inner He^{++} zone from the outer He^{+} one. It is caused by radiative transfer of

both direct and diffuse ionizing quanta in these objects and, probably, it is an important feature that can be used in the future to develop new methods for investigation of radial density distributions in such nebular environments using observed (integral over sightline) emission line intensities. From Figs. 1 and 2 it can be concluded that the He^{++} zone is also a little bit smaller in the case of *Detailed method* usage during PhM.

The decrease of the whole ionization volume of the nebular environment, as well as ionization zones of various ions, in the case of the usage of a more precise method for calculation of diffuse ionizing radiative transfer during PhM of these objects, led to the decrease of integral values of emissivities in emission lines. But how does it impact on the nebular integral emission line spectrum in the case of models of V1016 Cyg and HM Sge? To answer this question we gave in Table 2 the integral H_β luminosities and relative intensities for some important emission lines, obtained during PhM using the *Outward Only* approximation as well as the *Detailed method*. It can be seen from Table 2 that deviations of PhM results obtained using the approximate *Outward only* method from the ones calculated using the *Detailed method* are less than 2% for V1016 Cyg and less 1% in the case of HM Sge. Thus, these deviations are within the adopted precision for convergence of global integration (2%) and therefore we have concluded that the usage of the fast approximate *Outward only* method in Holovatyi et al. (2019) allowed us to obtain correct results which can be used in the future for more detailed investigations of symbiotic novae V1016 Cyg and HM Sge.

Acknowledgements. This work has been supported by a Grant 0118U003607 of the Ministry of Education and Science of Ukraine.

References

Arkhipova V.P., Taranova O.G., Ikonnikova N.P., Esipov V.F., Komissarova G.V., and Shenavrin V.I., Symbiotic nova V1016 Cygni: Evolution of the dust envelope and the gaseous nebula. 2015, *Astronomy Letters*, **41**, No.11, 613, DOI: 10.1134/S1063773715110018

Buhajenko O.S., Melekh B.Ya., Method for Detailed Calculation of the Diffuse Ionizing Radiation in Nebular Environments. 2016, *Journal of Physical Studies*, **20**, Issue 4, 4901

Buhajenko O.S., Melekh B.Ya., Photoionization modelling of planetary nebulae with realistic density distribution using detailed method for diffuse radiation calculation and Outward Only approximation. 2018, *Advances in Astronomy and Space Physics*, **8**, 3, DOI: 10.17721/2227-1481.8.3-8

Eyres S.P.S., Bode M.F., HST & VLA imaging of the symbiotic star HM Sge. 2001, in IAU Symposium, Vol. **205**, *Galaxies and their Consituents at the Highest Angular Resolutions*. ed. R.T. Schilizzi, 306–309, DOI: 10.1017/S007418090022130X

Ferland G.J., 2008, *Hazy, a Brief Introduction to Cloudy*, University of Kentucky: Physics Department Internal Report. See also: http://www.nublado.org and http://viewvc.nublado.org/index.cgi/tags/release/c08.00/docs/?root=cloudy

Golovatyi V. V., Malkov Y. F., Evolution of the Shells of Planetary Nebulae - an Empirical Approach. 1992, Soviet Astronomy, **36**, No.6/NOV, 599.

Holovatyi V. V., Melekh B. Ya.,Buhajenko O. S., Skulsky M. Yu. Physical and evolutionary characteristics of the symbiotic novae V1016 Cyg and HM Sge. 2018, *Journal of Physical Studies*, in press

Melekh B.Ya., Demchyna A.V., Holovatyi V.V., Envelope masses and distances to planetary nebulae: IC 5117 and NGC 7293. 2015, *Kinematics and Physics of the Celestial Bodies*, **31**, 2, 73, DOI: 10.3103/S088459131502004X

Muerset U., Nussbaumer H., Schmid H. M., & Vogel M., Temperature and luminosity of hot components in symbiotic stars. 1991, Astronomy & Astrophysics, **248**, 458.

Muerset U., & Nussbaumer H., Temperatures and luminosities of symbiotic novae. 1994, Astronomy & Astrophysics, **282**, 586.

Parimucha S., Chochol D., Pribulla T., Symbiotic Nova V1016 Cyg as Interacting Binary. 2001, *Odessa Astronomy Publications*, **14**, 61

Rudy R.J., Cohen R.D., Rossano G.S., & Puetter R.C., Optical and infrared spectrophotometry of the symbiotic system V1016 Cygni. 1990, *The Astrophysical Journal*, **362**, 346, DOI: 10.1086/169270

Sanad M.R., Ultraviolet spectroscopy of symbiotic nova V1016 Cyg with IUE and HST. 2017, *New Astronomy*, **52**, 14, DOI: 10.1016/j.newast.2016.10.002

Schmid H. M., Schild H., Physical conditions and elemental abundances in the symbiotic novae V1016 Cyg, HM Sge and HBV 475. 1990, Mon. Not. R. Astr. Soc., **246**, 84

Contrib. Astron. Obs. Skalnaté Pleso **49**, 503 – 521, (2019)

Photometric and spectroscopic investigation of nine Cepheids in the Cassiopeia constellation

J. Žák*[1,2], M. Skarka[1,2], E. Paunzen[1], P. Dubovský[3], M. Zejda[1] and G. Handler[4]

[1] *Department of Theoretical Physics and Astrophysics, Masaryk University, Kotlářská 2, CZ-611 37, Brno, The Czech Republic , (E-mail: 437396@mail.muni.cz)*

[2] *Astronomical Institute of the Czech Academy of Sciences 251 65 Ondřejov, The Czech Republic*

[3] *Vihorlat Astronomical Observatory, Mierová 4, SK-066 01 Humenné, The Slovak Republic*

[4] *Nicolaus Copernicus Astronomical Center, Bartycka 18, 00-716 Warsaw, Poland*

Received: August 9, 2019; Accepted: September 4, 2019

Abstract. We present new multicolor *BVRI* photometry and low-resolution spectroscopy of 9 fundamental mode Cepheids in the Cassiopeia constellation. Observations were carried out during the 2017/2018 observing season. We investigated each particular light curve in detail using Fourier decomposition techniques which we compare with the Cepheids from the OGLE project. Using the Gaia parallaxes and the period-luminosity relation we estimated the absolute magnitudes and constructed the Hertzsprung-Russell diagram. Our findings agree with the previously published results except for V824 Cas. This star has small Fourier amplitudes and shows a discrepancy in the absolute magnitudes based on Gaia and period-luminosity relation. We propose that V824 Cas can either be a member of a binary system or is not a fundamental-mode Cepheid but an overtone Cepheid.

Key words: Methods: Data Analysis – Techniques: Photometric – Techniques: Spectroscopic – Stars: Variables: Cepheids – Stars: Individual: V824 Cas

1. Introduction

Cepheids have played a prominent role in the history of astronomy. It was discovered that they change their brightness due to stellar pulsations (Shapley, 1914; Eddington, 1917). Leavitt & Pickering (1912) discovered the famous Period-Luminosity (P-L) relation, which ties the absolute magnitude with the pulsation period. This allows unprecedented distance measurements which makes Cepheids ideal objects for tracing the young population of the Milky Way Galaxy (Skowron et al., 2019; Benedict, McArthur, Feast, et al., 2007). Furthermore, classical Cepheids are the primary distance indicators for the extragalactic distance scale as they are used as standard candles. They provide a significant

contribution to the cosmic distance ladder as well as for the determination of the Hubble constant (Riess et al., 2018).

The typical Classical Cepheid is a young star with intermediate mass (3.5 to 15 $M_\odot$) which is a white-yellow population I supergiant (Catelan & Smith, 2015). Cepheids are radial pulsators which show periodic variations in radius, temperature, and brightness. The pulsation periods of Cepheids range from around 1 day to as long as 60 days. However, there are Cepheids observed in the Magellanic Clouds whose periods are longer than 100 days (Ulaczyk, Szymaski, Udalski, et al., 2013). The basic characterization of Cepheids can be performed by analysing their light curves. The shape of the light curves changes with the pulsation period. The amplitude of the light variations is wavelength dependent as it increases towards shorter wavelengths. Hertzsprung (1926) made the discovery that certain Cepheids show a relationship between the position of a bump on the light curve and the pulsation period. This phenomenon was named the "Hertzsprung progression".

Before the rapid growth of the automated surveys, such as OGLE (Udalski, Szymaski, Kaluzny, et al., 1992; Udalski, Szymański, & Szymański, 2015), ASAS-SN (Shappee, Prieto, Stanek, et al., 2014; Kochanek, Shappee, Stanek, et al., 2017) and many others, numerous observers (Szabados, 1981; Berdnikov, 2008) published multi-color observations of the Galactic Cepheids. These archival data have tremendous value as they can reveal evolutionary changes of the stars. The motivation of this work was to extend the time-base of multi-color observations for these stars.

The objective of this paper is to present new spectroscopic and *BVRI* photometric data of nine fundamental mode Cepheids in the Cassiopeia constellation (sect. 2). The analysis and description of the light curves using Fourier decomposition technique are presented in Sect. 4.1. The comparison with the OGLE Galactic Bulge Cepheids is in Sect. 4.2. The astrophysical parameters of the targets are investigated in Sect. 5. The possible origin of the unusual behavior of V824 Cas is discussed in Sect. 6. The summary is given in Sect. 7.

2. Observations

Photometry of Galactic Cepheids in the Cassiopeia constellation was performed from fall 2017 to summer 2018 using the 600/2780 mm Newtonian telescope (equipped with G4-16000 Moravian Instruments Peltier cooled CCD camera with Johnsons-Cousins *BVRI* filters) at Masaryk University Observatory (MUO), which is located in Brno, Czech Republic. The fundamental mode Cepheids were selected according to their location on the sky and their brightness to maximize the efficiency of the observations with the available equipment. The VSX catalog[1] (Watson, Henden, & Price, 2006) was used to eliminate Cepheids that were brighter than 10.3 magnitude in V-filter light maximum to ensure that the star

[1] https://www.aavso.org/vsx/

would not saturate with exposure times below 10 seconds. On the other hand, we omitted stars fainter than 11.8 mag in their V-filter light minimum to avoid exposure times above 90 s in B and to ensure a good signal to noise ratio. At last, we tried to select only stars that are apparently not blended. The selected stars together with the observing log are listed in Table 1. The photometric data are avaiable at
http://www.astro.sk/caosp/Eedition/FullTexts/vol49no3/pp503-521.dat/.

Table 1. Details to the investigated stars (taken from the VSX database). Cepheids are arranged according to increasing value of the pulsation period. The observation log presents the number of nights per star (#N) and the average number of frames per star in each of the filters (#f). The symbols in the last column are used in the forthcoming figures.

Star name	Sp. type	V [mag]	$(B\text{-}V)$ [mag]	#N	#f	
DF Cas	F6-G4	10.53 - 11.13	1.372	12	160	●
V395 Cas	G3	10.39 - 10.95	0.827	10	129	■
UZ Cas	F6-G2	10.93 - 11.73	1.082	13	127	▲
CG Cas	F5-F8	10.89 - 11.73	1.228	15	123	▼
CF Cas	F8Ib-G0Ib	10.80 - 11.47	1.156	15	136	◆
DW Cas	F7	10.81 - 11.41	1.288	8	82	▶
V824 Cas		11.03 - 11.36	1.272	11	89	◀
BP Cas	F6-G1	10.55 - 11.33	1.537	11	115	⋆
CH Cas	F3pIb-F6	10.47 - 11.56	1.755	13	57	⬟

Altogether, 4069 frames were obtained during 25 nights. All obtained frames were corrected for dark count and flat field using CMUNIPACK (Motl, 2011). Aperture photometry was also performed in CMUNIPACK. The star field containing CF Cas and CG Cas also contained a star cluster NGC 7790, which has been used for calibration to the standard system (Henden, 1999).

The spectroscopic observations (October and November 2018) were taken at the Astronomické observatórium na Kolonickom sedle (Slovak Republic) with a Schmidt-Cassegrain Celestron C11 telescope: aperture diameter 280 mm and an effective focal length of 1750 mm. The used LISA spectrograph (Shelyak) covers a wavelength region from 3 800 to 7 500 Å with a resolving power of about 1 000. The signal-to-noise ratios are between 50 and 100. The spectra are shown in Fig. 1.

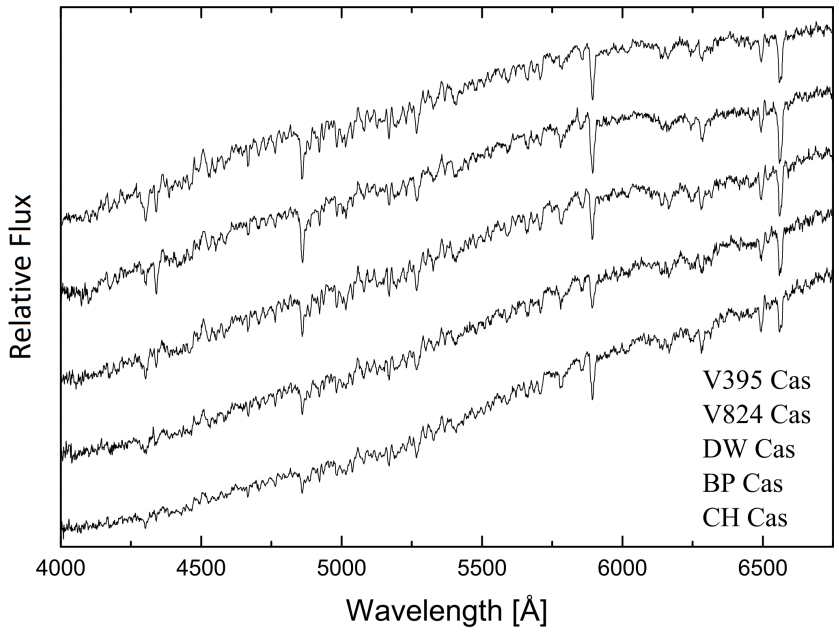

Figure 1. Classification resolution spectra of V824 Cas and four other investigated Cepheids of comparable spectral types.

3. Methods and analysis

3.1. New period determination

We have recalculated periods for all of the stars in our sample using ASAS-SN data. The PERSEA software (Maciejewski, 2007, based on the algorithm by Schwarzenberg-Czerny (1996)) was used to determine new periods. These calculations for each star were based on over 500 data points in a time range of approximately 1000 days. The periods can be found in Table 2. We show an example of the phase curves before and after recalculation of the period in Fig. 2 for V824 Cas. Note that the former period was based on data spanning only 13 days with typically 2 points per night.

3.2. Light curve fitting and Fourier coefficients

For the investigation of the light curves, we performed a fit with sine series

$$m(t) = A_0 + \sum_{i=1}^{N} a_i \ \cos(i\omega(t - t_0)) + \sum_{i=1}^{N} b_i \ \sin(i\omega(t - t_0)), \qquad (1)$$

Table 2. The periods of the sample stars. The second column shows the periods given in VSX. Newly calculated periods with the errors are given in the third column of the table.

Star name	Period in literature [d]	Calculated period [d]
DF Cas	3.832472	3.8324(5)
V395 Cas	4.037728	4.0380(5)
UZ Cas	4.259459	4.2595(6)
CG Cas	4.36554	4.3653(6)
CF Cas	4.87522	4.8750(7)
DW Cas	4.99776	4.9978(8)
V824 Cas	5.359	5.3507(9)
BP Cas	6.272724	6.272(1)
CH Cas	15.09215	15.098(7)

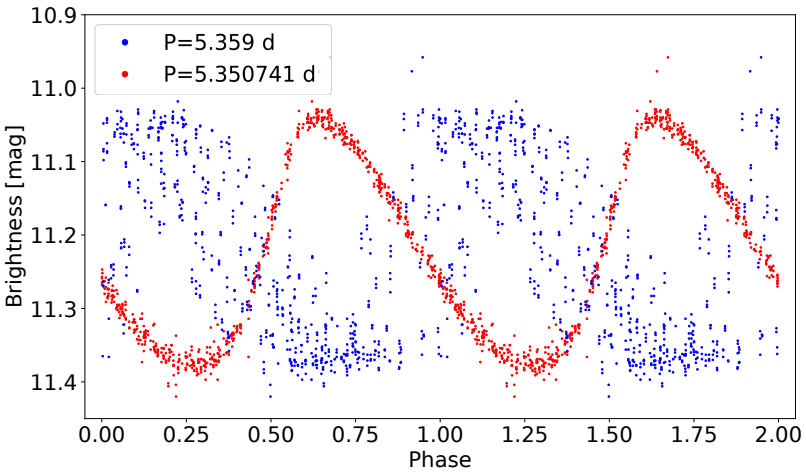

Figure 2. The comparison of the ASAS-SN data phased with former and newly determined period for V824 Cas.

where $m(t)$ is the observed magnitude at time t, A_0 is the mean magnitude, a_i, b_i are the amplitude components of the i-th harmonic, $\omega = 2\pi/P$ is the angular frequency, P is the period, N is the order of the series and t_0 is the epoch of maximum light.

The eq. 1 can also be written in the following more compact form that we

used in our analysis:

$$m(t) = A_0 + \sum_{k=1}^{N} A_k \ \sin(2\pi k \frac{(t-t_0)}{P} + \phi_k), \tag{2}$$

For all studied stars, we used a Fourier fit of the fourth order since it performed well in the visual test. Period P is presented at the bottom of each graph in Fig. 3.

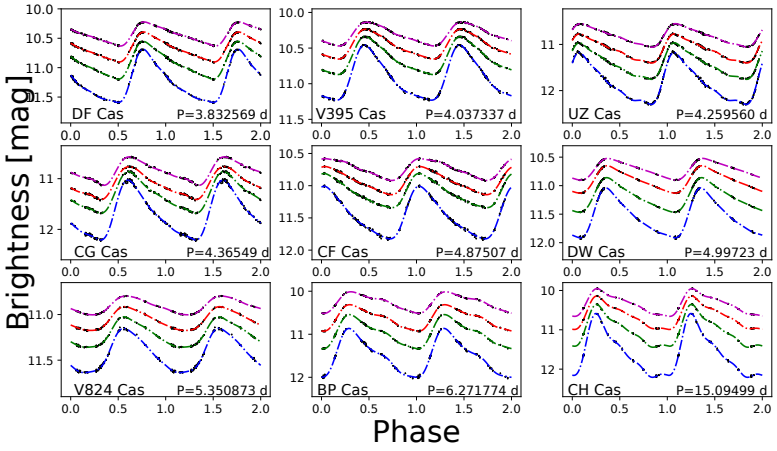

Figure 3. The phase curves of all studied stars. The phase curves are vertically shifted for a better visibility. Blue, green, red and magenta colors mark B, V, R and I filters respectively.

The light curves of well-observed Cepheids can be described by using Fourier coefficients, which were introduced by Schaltenbrand & Tammann (1971) and further developed by Simon & Lee (1981), who used it for studying structural properties of Cepheid light curves. These coefficients are defined as

$$R_{i1} = \frac{A_i}{A_1};\ \phi_{i1} = \phi_i - i\phi_1, \tag{3}$$

where amplitudes of the sine series are denoted with A and phases with ϕ. The index i is larger than 1.

4. Results

4.1. Amplitudes and Fourier Coefficients

We have used the ASAS-SN data (Shappee, Prieto, Stanek, et al., 2014; Kochanek, Shappee, Stanek, et al., 2017), and the Nitro database (Morgan, 2003) to compare our results with the other sources. The Nitro database contains data and Fourier coefficients for more than 1000 Galactic variables of which many are Cepheids. Except for V824 Cas[2], all studied stars are listed in this database. Data are in the V filter and are from different sources for all the stars. The data sources are listed in Table 3.

Table 3. The data sources for the Fourier coefficients in V filter.

Star	Source of data
DF Cas	Antonello, Poretti, & Reduzzi (1990)
UZ Cas	Antonello, Poretti, & Reduzzi (1990)
CG Cas	Antonello, Poretti, & Reduzzi (1990)
CF Cas	Moffett & Barnes (1985)
BP Cas	Simon & Lee (1981)
CH Cas	Antonello & Morelli (1996)
V824 Cas	Berdnikov (2008)

The comparison shows a good agreement for the majority of the stars (Fig. 4). One of the common reasons for the data discrepancy of the compared coefficients is the sparse coverage of the phase curves of data acquired at MUO. This is most noticeably apparent for CG Cas, DW Cas, and CH Cas (see the corresponding panels in Fig. 3). The discrepancy could also be caused by the different order of the Fourier fit and by the quality of the data from the literature. The data obtained at MUO are fitted with a Fourier fit of the fourth order. On the other hand, the order of the fit from the Nitro database varies from the third to the seventh order. Another cause can originate from various time bases of acquired data sets. The MUO data were obtained during roughly 10 months, ASAS-SN data were obtained during more than 30 months. These effects combined together preclude from obtaining results within the errorbar range.

From Fig. 3 it is apparent that the amplitude of the light curve is clearly wavelength dependent as it increases towards shorter wavelengths. Fig. 5 shows the pulsation amplitude of Cepheids in our sample in various passbands as a function of the pulsation period. Amplitudes and Fourier coefficients in all filters are listed in Tables 5-8 in the Appendix. V824 Cas exhibits unexpectedly low values of the amplitude for all filters when compared to the observations and the theoretical predictions shown in Bhardwaj, Kanbur, Marconi, et al. (2017).

[2]Data taken from Berdnikov (2008).

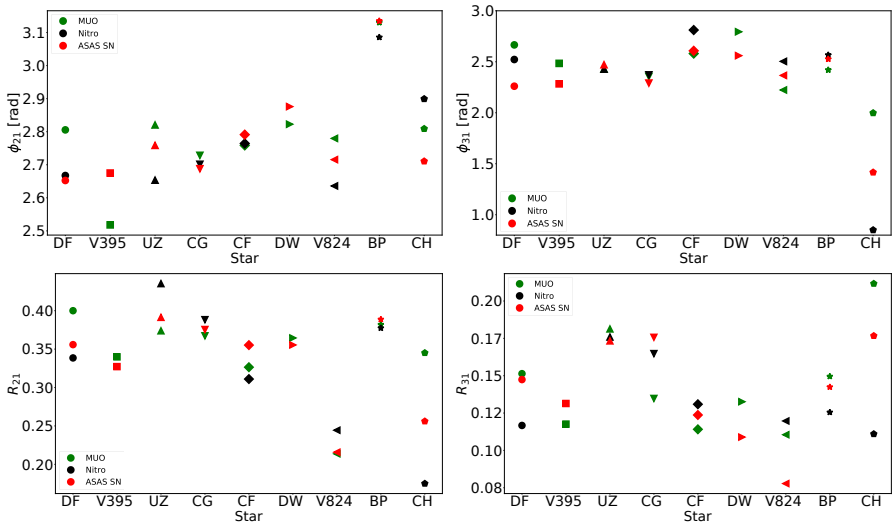

Figure 4. The comparison of Fourier coefficients to ASAS-SN data and to literature data. The symbols for the stars are the same as in Table. 1.

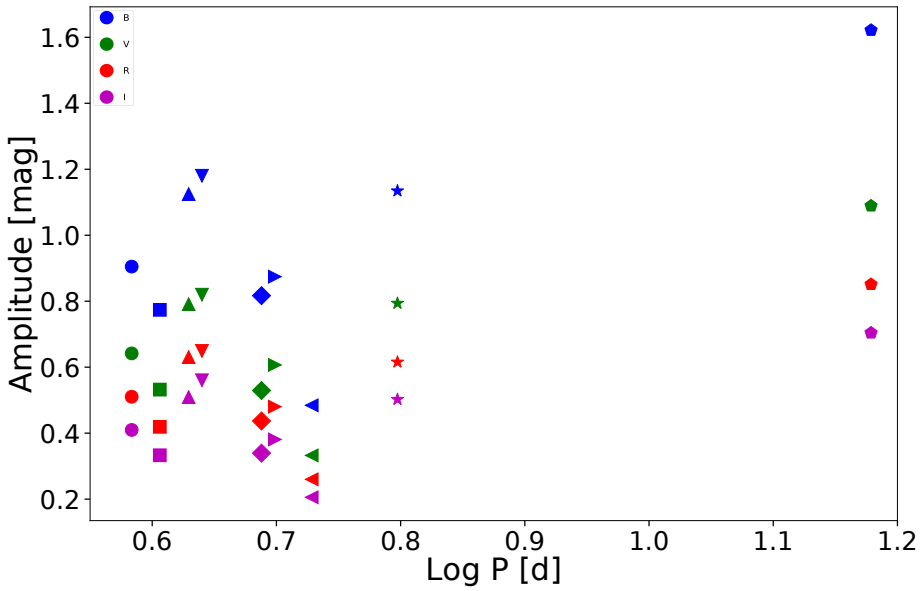

Figure 5. The light-curve amplitude dependency on the logarithm of the period for all filters. The symbols of the stars are defined in the last column of Table 1.

The Fourier parameters as a function of the pulsation period are shown in Fig. 6. The amplitude dependency on the wavelength results in clear dependency and systematics of ϕ_{21} and ϕ_{31} in different filters. However, the amplitude coefficients R_{21} and R_{31} lack this dependency (see Fig. 6).

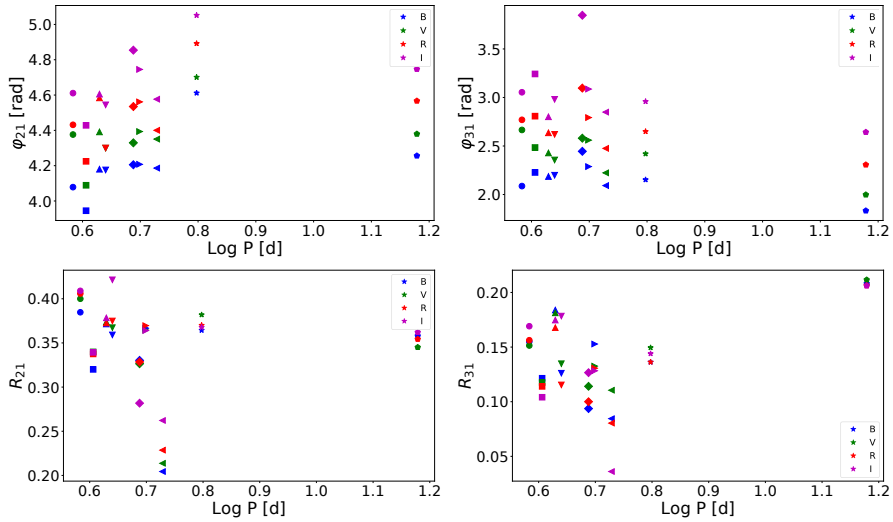

Figure 6. The obtained Fourier coefficients in different filters. The symbols of the stars are defined in the last column of Table 1

The period dependencies of obtained coefficients shown in Fig. 6 are in good agreement with the progressions predicted theoretically by Bhardwaj, Kanbur, Marconi, et al. (2017). The coefficient ϕ_{21} shows a clear rise with an increasing period from log(P) $\sim$ 0.6 d to log(P) $\sim$ 0.8 d. In Fig. 6, it can be seen that the coefficient ϕ_{31} is at the expected plateau which lasts from log(P) $\sim$ 0.6 d to log(P) $\sim$ 0.8 d.

The value of the R_{21} is not changing much. An exception is V824 Cas which shows significantly lower values of this coefficient (Fig. 6). Parameter R_{31} is slightly decreasing with increasing period until log(P) $\sim$ 0.8 d. Again, V824 Cas shows unexpectedly low values.

4.2. Comparison to OGLE data

The Optical Gravitational Lensing Experiment (OGLE, Udalski, Szymaski, Kaluzny, et al., 1992; Udalski, Szymański, & Szymański, 2015) is a survey with the main objective of searching for the dark matter with microlensing phenomena. As a byproduct, it has discovered several exoplanets (Bond et al., 2004) and created an enormous database of variable stars data. The main targets of in-

terest are specifically the Magellanic Clouds and the Galactic Bulge. Soszyński, Udalski, Szymaski, et al. (2015, 2017) have published an analysis of OGLE data and calculated Fourier coefficients for Cepheids in the Large and Small Magellanic Clouds (LMC and SMC) and the Galactic Bulge. We compare the Fourier coefficients in I filter from MUO and OGLE, because OGLE observations are made mostly in I filter[3]. The same markers for each star were used as originally in Table 1 are used in Fig. 7.

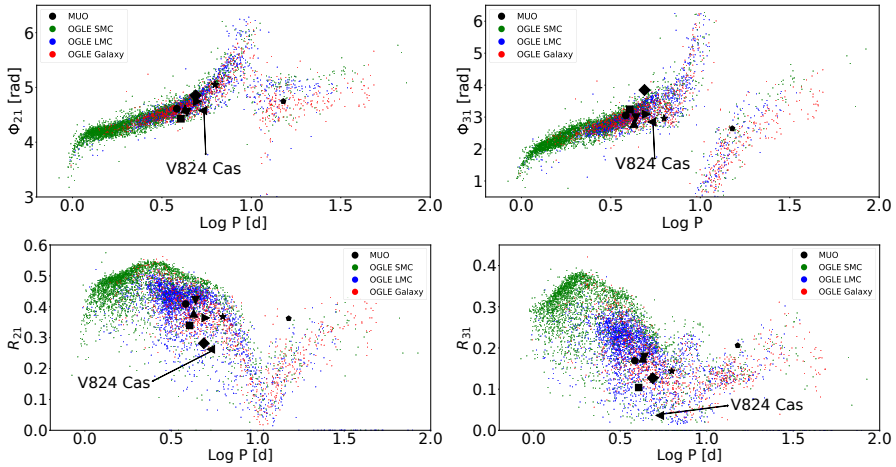

Figure 7. The comparison of the Fourier coefficients to OGLE Cepheids in the SMC, LMC and Galactic Bulge. The symbols for the stars are the same as in Tab. 1.

We can see a good agreement for most of the stars (Fig. 7). V824 Cas shows the largest deviation from the trends. The cause of the deviation towards lower values can have many origins: from data uncertainty to the physical origin. Literature data in Fig. 4 show even lower values than data obtained at MUO for ϕ_{21} and R_{31}. This may be an indication that the data are correct and V824 Cas could be a peculiar Cepheid.

Another star that differs from the general trends is CF Cas which has higher values of ϕ_{31} and lower values of R_{21} (Fig. 7). Coefficients from the literature (section 4.1) show a good agreement with the ones obtained at MUO, thus, we can conclude that the higher values are of a physical origin and not rather caused by the data uncertainty.

A very interesting is the comparison of R_{31} coefficient in Fig. 7 as there is a clear separation of Cepheids located in LMC, SMC, and Bulge. The value of the R_{31} coefficient decreases as the metallicity increases (Bhardwaj, Kanbur, Marconi, et al., 2017). The difference is because LMC, SMC and Galactic Bulge

[3]The coefficients were obtained from ftp://ftp.astrouw.edu.pl/ogle4/OCVS/

have different metallicity. The data from MUO nicely fits in this sequence when solar metallicity $Z = 0.02$ is used. $Z_{\rm SMC} = 0.004$ and $Z_{\rm LMC} = 0.008$ (Glatt, Grebel, & Koch, 2010). Stars located in the Galactic Bulge span metallicity range -1.5 $\lesssim$ [Fe/H] $\lesssim$ 0.5 (Barbuy, Chiappini, & Gerhard, 2018). This explains the widespread of values for OGLE Bulge Cepheids in the diagram.

5. Physical parameters

It is well known that Cepheids show a relatively wide range of effective temperatures (up to 1500 K) and thus colors during their pulsational phases (Fernley, Skillen, & Jameson, 1989). Therefore, we use here mean colors for all objects. The reddening values and metallicities were taken from the paper by Groenewegen (2018) whereas the mean *(B - V)* and V values were taken from the catalog by Fernie, Beattie, Evans, et al. (1995). Only one star, V824 Cas, is not included in these references. For this object, the BV magnitudes were taken from Kharchenko (2001). This all-sky catalogue of more than 2.5 million stars transformed the Hipparcos/Tycho BV magnitudes in standard Johnson ones, using a homogenized transformation law. The reddening value was interpolated within the corresponding maps published by Green, Schlafly, Finkbeiner, et al. (2018) using the range of distances from the Gaia DR2 (Bailer-Jones et al., 2018). We also compared the published reddening values of the other targets from Groenewegen (2018) with the reddening map which yields an excellent agreement.

To estimate the absolute magnitudes of our targets, we used the *PLZ* relation from Groenewegen (2018) and the basic approach applying the parallaxes from the Gaia DR2 (Lindegren, Hernández, Bombrun, et al., 2018). We compared the absolute magnitudes from three different *PLZ* relations using V, K, and the reddening-free Wesenheit index. The results of all three relations are in excellent agreement from which we conclude that the photometry is consistent and that the reddening values are correct. The errors of the absolute magnitudes were calculated with a full propagation of uncertainties, i.e. the parallax errors and the V amplitudes as listed in Table 6.

We checked, if the metallicities of our targets deviate significantly from the solar. In a series of papers, Andrievsky, Luck, Korotin (2014) published detailed abundances of Cepheids. All but V824 Cas are included in these papers. Two stars, CH Cas and DF Cas, are slightly overabundant (about 0.2 dex) in [Fe/H]. Using these metallicities and using the corresponding *PLZ* relation from Groenewegen (2018), the difference to the absolute magnitude from the *PLZ* relation is only 0.04 mag, respectively. This is negligible compared to the other error sources.

The parallaxes, colors, reddening values, and absolute magnitudes together with their errors are listed in Tab. 4. The comparison of the absolute magnitudes shows that only V824 Cas is outstanding with non-compatible values. This fits

Table 4. Parallaxes, colors, reddening values, and absolute magnitudes for our our targets. The latter were derived from the parallaxes (M_V^{Gaia}) and the PL relation (M_V^{PL}) taken from Groenewegen (2018).

Star name	Parallax [mas]	*(B - V)* [mag]	*E(B - V)* [mag]	M_V^{Gaia} [mag]	M_V^{PL} [mag]
DF Cas	0.307(28)	1.181	0.564(499)	-3.45(38)	-3.31(20)
V395 Cas	0.247(68)	1.146	0.565(56)	-4.05(65)	-3.37(20)
UZ Cas	0.149(30)	1.110	0.469(34)	-4.22(59)	-3.42(21)
CG Cas	0.224(30)	1.250	0.667(9)	-3.95(50)	-3.45(21)
CF Cas	0.287(32)	1.174	0.556(21)	-3.28(36)	-3.56(21)
DW Cas	0.355(26)	1.475	0.807(32)	-3.62(35)	-3.59(22)
V824 Cas	0.206(28)	1.272	0.810(50)	-4.87(34)	-3.66(22)
BP Cas	0.374(28)	1.550	0.864(14)	-3.86(43)	-3.82(23)
CH Cas	0.271(28)	1.650	0.942(36)	-4.73(59)	-4.73(28)

very well in the peculiar light curve parameters (see Sect. 4.1). This star is discussed in Sect. 6.

As the last step, we located our targets in $(B - V)_0$ versus M_V diagram in order to check if they populate the known Cepheid domain. In Fig. 8 the results are plotted together with the solar-abundance ($[Z] = 0.019$) isochrones taken from the PARSEC database (Bressan, Marigo, Girardi, et al., 2012).

It is well known that a star may cross the Cepheid instability strip on the Hertzsprung-Russell (HR) diagram more than once during its evolution. After the exhaustion of hydrogen in the core, it expands to become a red giant and then crosses the instability strip rapidly on a Kelvin-Helmholtz time scale. It climbs the red giant branch to the red giant tip and after the ignition of helium burning in the core (a relatively long-lived evolutionary stage) it may make a loop to a higher temperature in the HR diagram. As can be seen from Fig. 8 our targets may cover these two different evolutionary stages with ages between 40 and 100 Myr, respectively. Again, V824 Cas is outstanding because it is brighter than normal Cepheids for the given color and period. We note that the pulsation phase at which the input values were taken for V824 Cas is unknown, thus, possibly introducing further uncertainty in HRD position.

6. Origin of the peculiar behavior of V824 Cas

It is seen in Fig. 5 that V824 Cas exhibits unexpectedly low amplitudes in all photometric bands. The unusually low amplitudes of V824 Cas brings up the question of whether the Cepheid is correctly classified.

A special class of Cepheids, the so-called s-Cepheids (sometimes called DCEPS), are delta Cephei variables with photometric amplitude below 0.5 mag in V (0.7 mag in B) and almost symmetrical light curves, their period is usually shorter than $P < 7$ d (Samus' et al., 2017). Most likely they are first-overtone pulsators. First overtone Cepheids follow different P-L relation than the funda-

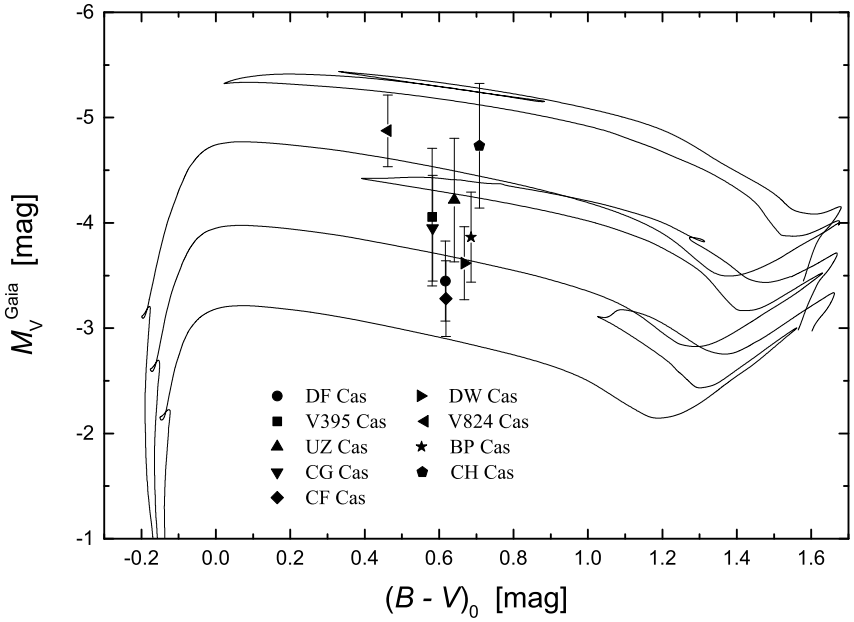

Figure 8. The *(B - V)₀* versus M_V diagram of our program stars together with the solar-abundance ([Z] = 0.019) isochrones ($\log t = 8.0$, 7.8, and 7.6) taken from the PARSEC database (Bressan, Marigo, Girardi, et al., 2012).

mental ones (Udalski et al., 1999) as they are brighter for a given period. As can be seen in the Fig. 8 V824 Cas has high luminosity which is suggesting overtone nature.

The methodology described in a paper by Antonello, Poretti, & Reduzzi (1990) gives two suitable criteria to distinguish the s-Cepheids from their normal amplitude relatives using the Fourier parameters. S-Cepheids should form a lower sequence below the normal amplitude Cepheids sequence in the R_{21} versus pulsation period plot. Another criterion was postulated as the s-Cepheids should form an upper sequence above the normal amplitude Cepheids in the ϕ_{31} versus period plot.

It can be seen that the first criterion is met, however, the second has failed (Fig. 6). Thus, the classification of V824 Cas as s-Cepheid is not conclusive. Turner, Usenko, & Kovtyukh (2006) have shown that a sinusoidal light curve is not a conclusive evidence for overtone pulsations and that high-resolution spectroscopic observations are needed to determine the pulsation mode.

Another explanation for the unusual amplitude can be a binary status. Binarity plays a relevant role when investigating the observed amplitudes of Cepheids, as more than 50 % of the Galactic Cepheids belong to binary or mul-

tiple systems (Szabados, 2003). The presence of a companion can affect the photometric amplitudes and cause a reduction of the observable amplitude of the brightness variation due to the presence of a constant source of light. This was used in a paper by Coulson & Caldwell (1989) on the sample of Cepheids to hint a possibility of a hidden companion for Cepheids that deviate from a constant trend.

We have investigated the RUWE [4] coefficient ϱ computed in Gaia DR2 (Gaia Collaboration et al., 2018; Lindegren, Hernández, Bombrun, et al., 2018). Values above $\varrho > 1.4$ can hint a possible binarity. However, all Cepheids in our sample have values between 0.85 and 1.07. A known spectroscopic binary Cepheid in our sample CG Cas (Szabados, 1996) has a value of $\varrho = 0.981$. Also, we have compared the Gaia DR2 parallax errors in Table 4 to check for any deviations. Only V395 Cas has double the parallax error compared to the other stars, also possibly hinting a companion presence.

As shown by Tanvir (1997) the amplitude ratio A_I/A_V is not dependent on the period and has a constant value of $A_I/A_V \sim 0.64$. V824 Cas exhibits deviation from this value, which might imply the presence of a companion. This finding deserves further, more complex, both photometric and spectroscopic investigations as there are no spectroscopic measurements available in the literature. It is worth to mention that the Gaia DR2 catalog data do not suggest the presence of a visual companion that could affect the amplitude.

Unusually high metallicity of V824 Cas might be another explanation of its unexpected behavior. The amplitude coefficient R_{31} is metallicity dependent so that with an increasing metallicity the value of R_{31} decreases (Fig. 7). Since no abundance estimates for V824 Cas are available in the literature, we compared our classification resolution spectra of all targets in order to search for any significant enhancements. In Fig. 1, five spectra are plotted. The metallic line spectrum of V824 Cas is comparable to those of the other four targets. We can, therefore, rule out this scenario.

7. Summary and conclusions

We present an analysis of DF Cas, V395 Cas, UZ Cas, CG Cas, CF Cas, DW Cas, V824 Cas, BP Cas and CH Cas based on new *BVRI* photometry and low-resolution spectroscopy. The observations were carried out during 25 nights in 2017/2018 using 600-mm telescope at Masaryk University Observatory, Brno, Czech Republic (photometry) and Astronomické observatórium na Kolonickom sedle, Slovak Republic (spectroscopy).

We have performed new period determinations for all the stars in our sample as previous data were obsolete or not precise enough. The photometric data were fitted with a Fourier fit of the fourth-order to obtain the Fourier coefficients. By

[4] https://www.cosmos.esa.int/web/gaia/dr2-known-issues

comparing our results with those from the literature we find no major deviations except for V824 Cas which shows unusually low amplitudes.

Employing the Gaia DR2 parallaxes and available photometric measurements and reddening maps we estimated the absolute magnitudes of the sample Cepheids and constructed an HR diagram. We found that all the targets are located within the classical Cepheid instability strip with ages between 40 and 100 Myr. Except for V824 Cas, the absolute magnitudes based on the parallaxes and the *PL* relations are in agreement within the error bars. This behavior also points towards a peculiarity of V824 Cas.

V824 Cas appears to have an extraordinary low pulsation amplitude and amplitude Fourier coefficients compared to other Cepheids. From a comparison with literature data and parameters based on the ASAS-SN photometry, we can exclude an instrumental origin of the peculiarity. We propose two possible explanations of the peculiar behavior. V824 Cas could either be an s-Cepheid (DCEPS) or a classical Cepheid in a binary system. We recommend to obtain a high-resolution spectroscopic data to solve the status of V824 Cas.

Acknowledgements. JZ would like to acknowledge the support from the Rector's program of Masaryk University (MUNI/C/1675/2018). MS acknowledges the financial support of Postdoc@MUNI project CZ.02.2.69/0.0/0.0/16_027/0008360. GH's work and the spectrograph used in this study were funded by the Polish NCN grant 2015/18/A/ST9/00578. We would like to thank the anonymous referee for careful reading and providing comments that helped to improve the manuscript.

References

Andrievsky S. M., Luck R. E., Korotin S. A.: 2014, *Mon. Not. R. Astron. Soc.* **437**, 2106

Antonello E., Morelli P. L.: 1996, *Astron. Astrophys.* **314**, 541

Antonello E., Poretti E., Reduzzi L.: 1990, *Astron. Astrophys.* **236**, 138

Bailer-Jones C. A. L., Rybizki J., Fouesneau M., Mantelet G., Andrae R.: 2018, *Astron. J.* **156**, 58

Barbuy, B., Chiappini, C., & Gerhard, O. 2018, *Ann. Rev. Astron. Astrophys.* **56**, 223

Benedict G. F., McArthur B. E., Feast M. W., et al.: 2007, *Astron. J.* **133**, 1810

Berdnikov, L. N.: 2008, *VizieR Online Data Catalog* **2285**

Bhardwaj A., Kanbur S. M., Marconi M., et al.: 2017, *Mon. Not. R. Astron. Soc.* **466**, 2805

Bond, I. A., Udalski, A., Jaroszyński, M., et al.: 2004, *Astrophys. J., Lett.* **606**, L155

Bressan A., Marigo P., Girardi L., et al.: 2012, *Mon. Not. R. Astron. Soc.* **427**, 127

Catelan M., Smith H. A., 2015, *Pulsating stars*, Wiley-VCH, United States

Coulson I. M., Caldwell J. A. R.: 1989, *Mon. Not. R. Astron. Soc.* **240**, 285

Eddington A. S.: 1917, *Observatory* **40**, 290

Fernie J. D., Beattie B., Evans N. R., Seager S.: 1995, *Inf. Bull. Variable Stars* **4148**, 1

Fernley J. A., Skillen I., Jameson, R. F.: 1989, *Mon. Not. R. Astron. Soc.* **237**, 947

Gaia Collaboration, Brown, A. G. A., Vallenari, A., et al.: 2018, *Astron. Astrophys.* **616**, A1

Glatt K., Grebel E. K., Koch A.: 2010, *Astron. Astrophys.* **517**, A50

Green G. M., Schlafly E. F. Finkbeiner D.: 2018, *Mon. Not. R. Astron. Soc.* **478**, 651

Groenewegen M. A. T.: 20018, *Astron. Astrophys.* **619**, A8

Henden A.: 1999, *online*
http://binaries.boulder.swri.edu/fields/ngc7790.html

Hertzsprung E.: 1926, *Bull. Astron. Inst. Netherlands* **3**, 115

Kharchenko N. V.: 2001, *Kinematika i Fizika Nebesnykh Tel* **17**, 409

Kochanek C. S., Shappee B. J., Stanek K. Z., et al.: 2017, *Publ. Astron. Soc. Pac.* **129**, 104502

Leavitt H. S., Pickering E. C., et al.: 1912, *Harvard Circ.* **173**, 1

Lindegren L., Hernández J., Bombrun A., et al.: 2018, *Astron. Astrophys.* **616**, A2

Maciejewski G.: 2007, *online* PerSea,
http://www.astri.uni.torun.pl/

Moffett T. J., Barnes T. G., III, et al.: 1985, *Astrophys. J., Suppl.* **58**, 843

Morgan S.: 2003, *online* Nitro database,
http://nitro9.earth.uni.edu/

Motl D.: 2011, *online* CMuniPack,
http://c-munipack.sourceforge.net/

Riess, A. G., Casertano, S., Yuan, W., et al.: 2018, *Astrophys. J.* **861**, 12

Samus' N. N., Kazarovets E. V., Durlevich O. V., Kireeva N. N., Pastukhova E. N.: 2017, *Astronomy Reports* **61**, 80

Schaltenbrand R., Tammann G.: 1971, *Astron. Astrophys., Suppl. Ser.* **4**, 265

Schwarzenberg-Czerny A.: 1996, *Astrophys. J.* **460**, L107

Shapley H.: 1914, *Astrophys. J.* **40**, 448

Shappee B., Prieto J., Stanek K.Z., et al.: 2014, *American Astronomical Society* **223**, 236.03

Simon N. R., Lee A. S.: 1981, *Astrophys. J.* **248**, 291

Skowron, D. M., Skowron, J., Mróz, P., et al.: 2019, *Science* **365**, 478

Soszyski I., Udalski A., Szymaski M.K., et al.: 2015, *Acta Astron.* **65**, 297

Soszyski I., Udalski A., Szymaski M.K., et al.: 2017, *Acta Astron.* **67**, 297

Szabados, L.: 1981, *Commmunications of the Konkoly Observatory* **77**, 1

Szabados L.: 1996, *Astron. Astrophys.* **311**, 189

Szabados L.: 2003, *Inf. Bull. Variable Stars* **5394**, 1

Tanvir N. R.: 1997, *EDS proceedings* **91**

Turner D. G., Usenko I. A., Kovtyukh V. V.,: 2006, *Observatory* **126**, 207

Udalski A., Szymaski M., Kaluzny J., et al.: 1992, *Acta Astron.* **42**, 253

Udalski, A., Szymanski, M., Kubiak, M., et al.: 1999, *Acta Astron.* **49**, 201

Udalski A., Szymański M. K., Szymański G.: 2015, *Acta Astron.* **65**, 1

Ulaczyk K., Szymaski M. K., Udalski A., et al.: 2013, *Acta Astron.* **63**, 159

Watson C. L., Henden A. A., Price A.: 2006, *Society for Astronomical Sciences Annual Symposium* **25**, 47

A. Appendix

Table 5. Amplitude and Fourier coefficients of the sample Cepheids in B filter. Values in the parenthesis are obtained errors.

Star	A [mag]	A_0 [mag]	A_1 [mag]	R_{21}	R_{31}	R_{41}	Φ_1 [rad]	Φ_{21} [rad]	Φ_{31} [rad]	Φ_{41} [rad]
DF Cas	0.91	12.133(1)	0.386(2)	0.385(4)	0.155(5)	0.075(6)	0.842(4)	2.508(17)	5.228(30)	1.643(63)
V395 Cas	0.77	11.918(1)	0.352(2)	0.320(4)	0.121(4)	0.036(4)	3.609(4)	2.374(18)	5.369(43)	1.43(14)
UZ Cas	1.13	12.488(3)	0.474(4)	0.371(7)	0.184(10)	0.104(7)	2.276(7)	2.609(29)	5.327(42)	2.074(73)
CG Cas	1.18	12.605(4)	0.514(3)	0.359(7)	0.126(7)	0.037(5)	1.025(14)	2.605(42)	5.340(75)	2.48(23)
CF Cas	0.82	12.369(1)	0.365(2)	0.330(6)	0.094(5)	0.303(5)	2.212(5)	2.634(16)	5.587(56)	2.02(17)
DW Cas	0.87	12.647(1)	0.375(4)	0.367(13)	0.150(13)	0.056(11)	1.173(11)	2.637(37)	5.429(70)	1.99(17)
V824 Cas	0.48	12.475(2)	0.235(2)	0.204(8)	0.085(13)	0.043(11)	4.798(8)	2.615(54)	5.234(89)	1.89(21)
BP Cas	1.13	12.502(2)	0.491(4)	0.364(6)	0.136(6)	0.051(10)	1.840(5)	3.041(23)	5.294(47)	2.53(10)
CH Cas	1.62	12.752(5)	0.671(7)	0.358(18)	0.208(9)	0.133(12)	0.328(14)	2.625(34)	4.98(10)	1.38(12)

Table 6. Amplitude and Fourier coefficients for the sample Cepheids in V filter.

Star	A [mag]	A_0 [mag]	A_1 [mag]	R_{21}	R_{31}	R_{41}	Φ_1 [rad]	Φ_{21} [rad]	Φ_{31} [rad]	Φ_{41} [rad]
DF Cas	0.64	10.906(1)	0.265(1)	0.400(4)	0.151(5)	0.067(6)	0.712(5)	2.805(17)	5.807(33)	2.340(65)
V395 Cas	0.53	10.644(1)	0.237(1)	0.340(4)	0.118(4)	0.042(4)	3.509(5)	2.518(19)	5.626(46)	1.91(13)
UZ Cas	0.79	11.415(2)	0.330(3)	0.374(8)	0.181(10)	0.108(8)	2.184(7)	2.820(33)	5.570(47)	2.312(77)
CG Cas	0.82	11.317(3)	0.349(2)	0.367(7)	0.135(7)	0.022(6)	0.961(14)	2.729(41)	5.498(70)	3.01(38)
CF Cas	0.53	11.104(1)	0.237(1)	0.326(6)	0.114(6)	0.056(5)	2.120(5)	2.759(18)	5.722(49)	2.349(98)
DW Cas	0.61	11.197(1)	0.259(2)	0.364(10)	0.133(8)	0.041(8)	1.083(7)	2.823(24)	5.702(64)	1.99(18)
V824 Cas	0.33	11.213(1)	0.159(1)	0.214(6)	0.111(9)	0.041(7)	4.742(6)	2.780(37)	5.365(57)	1.65(19)
BP Cas	0.79	10.970(1)	0.335(2)	0.382(5)	0.150(4)	0.049(8)	1.293(4)	3.130(16)	5.561(32)	3.135(71)
CH Cas	1.09	11.019(3)	0.454(5)	0.345(17)	0.212(6)	0.138(11)	0.226(13)	2.809(31)	5.139(95)	1.712(98)

Table 7. Amplitude and Fourier coefficients of the sample Cepheids in R filter.

Star	A [mag]	A_0 [mag]	A_1 [mag]	R_{21}	R_{31}	R_{41}	Φ_1 [rad]	Φ_{21} [rad]	Φ_{31} [rad]	Φ_{41} [rad]
DF Cas	0.51	10.469(1)	0.209(1)	0.406(6)	0.156(7)	0.068(8)	0.650(7)	2.861(22)	5.911(44)	2.510(87)
V395 Cas	0.42	10.064(1)	0.186(1)	0.338(5)	0.114(5)	0.046(5)	3.431(6)	2.664(23)	5.949(58)	2.29(14)
UZ Cas	0.63	10.814(2)	0.264(3)	0.373(9)	0.168(11)	0.119(8)	2.100(8)	3.013(35)	5.778(56)	2.666(79)
CG Cas	0.65	10.807(3)	0.275(2)	0.375(8)	0.115(8)	0.045(8)	0.943(16)	2.729(45)	5.761(90)	3.76(17)
CF Cas	0.44	10.628(1)	0.193(1)	0.328(7)	0.100(7)	0.034(6)	2.031(6)	2.964(21)	6.238(67)	2.59(18)
DW Cas	0.48	10.407(1)	0.203(2)	0.37(11)	0.131(9)	0.044(8)	0.991(8)	2.990(26)	5.935(73)	2.31(18)
V824 Cas	0.26	10.456(1)	0.124(1)	0.229(7)	0.080(10)	0.033(9)	4.695(8)	2.829(41)	5.617(86)	1.88(26)
BP Cas	0.62	10.126(1)	0.264(1)	0.370(4)	0.136(4)	0.065(7)	1.375(4)	3.321(15)	5.791(31)	3.557(51)
CH Cas	0.85	10.044(2)	0.359(3)	0.354(12)	0.206(5)	0.123(9)	0.134(9)	2.996(23)	5.449(69)	2.074(85)

Table 8. Amplitude and Fourier coefficients of the sample Cepheids in I filter.

Star	A [mag]	A_0 [mag]	A_1 [mag]	R_{21}	R_{31}	R_{41}	Φ_1 [rad]	Φ_{21} [rad]	Φ_{31} [rad]	Φ_{41} [rad]
DF Cas	0.41	9.631(1)	0.166(1)	0.409(5)	0.169(6)	0.086(8)	0.530(7)	3.040(21)	6.195(40)	3.011(61)
V395 Cas	0.33	9.388(1)	0.147(1)	0.339(5)	0.104(6)	0.048(5)	3.311(7)	2.858(25)	0.101(65)	2.84(15)
UZ Cas	0.51	10.117(1)	0.211(2)	0.378(8)	0.175(10)	0.092(8)	2.029(7)	3.035(33)	5.943(53)	2.955(90)
CG Cas	0.56	9.850(3)	0.223(2)	0.421(11)	0.178(10)	0.057(8)	0.742(20)	2.974(53)	6.122(84)	3.70(23)
CF Cas	0.34	9.718(1)	0.155(1)	0.281(6)	0.127(6)	0.044(5)	1.886(6)	3.284(21)	0.706(44)	2.61(13)
DW Cas	0.38	9.514(1)	0.162(2)	0.364(16)	0.128(20)	0.044(17)	0.887(17)	3.174(63)	6.23(0.11)	2.94(26)
V824 Cas	0.21	9.554(1)	0.097(1)	0.262(6)	0.036(7)	0.037(8)	4.607(6)	3.006(29)	5.99(15)	2.69(15)
BP Cas	0.5	9.156(1)	0.214(1)	0.368(5)	0.144(5)	0.043(7)	1.477(5)	3.481(17)	6.101(33)	4.19(11)
CH Cas	0.7	8.945(2)	0.292(4)	0.362(16)	0.206(7)	0.117(12)	0.032(11)	3.176(28)	5.784(92)	2.53(12)

Contrib. Astron. Obs. Skalnaté Pleso **49**, 522 – 527, (2019)

Observational astrophysics: from proposals to publication

P. Kabath[1], H. Korhonen[2] and D. Jones[3,4]

[1] *Astronomical Institute of the Czech Academy of Sciences 251 65 Ondřejov, The Czech Republic, (E-mail: petr.kabath@asu.cas.cz)*

[2] *DARK, Niels Bohr Institute, University of Copenhagen, Lyngbyvej 2, DK-2100 Copenhagen, Denmark*

[3] *Instituto de Astrofsica de Canarias, E-38205 La Laguna, Tenerife, Spain*

[4] *Universidad de La Laguna, E-38206 La Laguna, Tenerife, Spain*

Received: September 26, 2019; Accepted: October 10, 2019

Abstract. The education of early career researchers in astronomy is growing in importance, as new and complex instruments are being commissioned to pioneer new hot topics in astrophysical research. Young researchers usually do not have the opportunities to gain hands-on experience with instrumentation and the telescope time application process in their early careers. To help provide such opportunities, ERASMUS+ and OPTICON joined forces and organised two summer schools in one event held at Stará Lesná in Slovakia between 17 and 27 July in 2019. Here, we describe the school and results of student group work which offered a high quality scientific output obtained in a short time.

Key words: Astronomical instrumentation, methods and techniques – Methods: data analysis

1. Introduction

Education of early career researchers is more and more demanding with the development of new instruments and with operations of new and modern observatories producing large amounts of data. Students usually have only limited opportunities to gain experience with these new instruments and novel methods. A natural way to improve the careers of young researchers is their participation in various summer schools, where the data reduction skills, new observing techniques and instrumentation development are presented. This is very well illustrated in a recent Astro2020 White Paper on the importance of telescope training for young astronomers (Whelan et al., 2019).

2. Early career education programmes in astronomy

The traditional organiser of such summer/winter schools is OPTICON (Optical Infrared Coordination Network for Astronomy) with a series of NEON Observing Schools and other schools in observational astrophysics. OPTICON is a

large EU-funded Research and Innovation project that has been running since the EU funding period FP6. It consists of three main areas: joint research activities, trans-national access, and networking activities. OPTICON has 16 work packages and WP12 *Enhancing community skills, Integrating communities* is a networking activity that is dedicated to organising schools in different aspects of observational astrophysics.

The key goals for the OPTICON WP12 are: 1) training of early career researchers in optical and infra-red observing techniques and data reduction procedures, 2) advancing the knowledge of astronomical instrumentation at all career stages, and 3) enabling equal participation of all EU member states in new large scale facilities. These goals are reached by organising 2–3 schools and workshops every year. The events include NEON Observing schools providing hands-on observing experience at professional telescopes, instrumentation schools, and Hot Topics conferences[1].

ERASMUS+ is an EU funded programme which promotes mobility of students, teachers and researchers and it is divided into Key Actions. Astronomical institute of Czech Academy of Sciences obtained an ERASMUS+ KA2 grant 2017-1-CZ01-KA203-035562 titled: "Per Aspera ad Astra Simul" with international partners from Instituto de Astrofisica de Canarias (IAC), Spain, Masaryk University, Czech Republic, Comenius University, Slovakia, Astronomical Institute of Slovak Academy of Sciences and with an associated partner Gran Telescopio de Canarias, Spain. Our project consists of two parts, firstly it enables a short term mobility of experienced researchers between partner institutes and secondly, it allows for long term mobility (up to 12 months) of early career researchers who can spend their time enhancing their careers at partner institutes.

One of the goals of our ERASMUS+ project is to disseminate the results of new educational and scientific approaches developed during the exchanges. As a dissemination event, a summer school on Observing techniques and data reduction of astrophysical data was organised. In order to make for a more complete experience, the data reduction school was joined with proposal writing school organised by OPTICON. The two schools strongly and logically connected, covering the needs of students to gain experience with modern data and instrumentation but also with proposal writing and the telescope time allocation process, with the latter becoming more and more competitive.

3. Joint ERASMUS+ and OPTICON summer schools

These two different EU funded programmes were united in the school "Observational Astrophysics: from proposals to publication" which was held at AI SAV at Stará Lesná in Slovakia between 17 and 27 July in 2019. In total, 28 students from 12 EU countries and associated states as well as one student from Ethiopia

[1]You can find more information on the OPTICON organised schools at https://opticon-schools.nbi.ku.dk/

participated. Unfortunately, two students from Morocco could not obtain visa in time, even if though their applications were made one month before the school.

The different aspects of the school will be introduced in detail in the following sections, while the results from students' projects will be presented in form of conference proceedings.

4. Data reduction part of the school

The first part was dedicated to lectures introducing various observatories and also OPTICON and ERASMUS+ programmes. Besides lectures (taking place mostly on 18 June), about 30 hours of group work was planned for students. After the talk about European Southern Observatory, the first hands-on session dealing with photometric data reduction was presented by H. M. J. Boffin (ESO) and prepared by D. Jones (IAC). The 28 students were then divided into groups led by experienced tutors from partner institutes. These groups consisted of 4–5 students working on a particular hot topic in modern astronomy such as quasars, exoplanets, Solar system bodies and AGNs. The group work comprised reading up on the topic proposed by the tutor and to then reduce and analyse a selected data set. Furthermore, the results of the students' analyses later presented on Sunday 24 June during a closing mini-conference. Each group had 15 minutes for their talk and 5 minutes for questions. The whole process very precisely simulated a real scientific conference and thus young participants also has the opportunity to improve their presenting skills. Each project and its results will be presented as an article of this proceedings.

A session on "How to write a good paper" was remotely presented by P. Woods, editor of Nature Astronomy. After the scientific paper writing session, a career session was opened by H. Korhonen who summarised the most important things for a successful career in astronomy (and science, in general). Subsequently, an extensive discussion about careers and paper writing opened. Students wanted to know how to deal with the referee reports as well as career aspects such as how to obtain a position or how a scientific career can be successfully combined with family life.

In general, the school allowed students to gain first-hand experience with modern data reduction processes for spectroscopic and photometric data. Furthermore, the importance of data archives and various routines for data analyses other than common IRAF [2] were also presented to the students. A relatively large number of hours (about 30) were dedicated to group work, allowing for detailed and careful analysis and ultimately for the preparation of high quality presentations.

[2]IRAF is distributed by the National Optical Astronomy Observatory, which is operated by the Association of Universities for Research in Astronomy (AURA) under a cooperative agreement with the National Science Foundation.

5. Proposal - time allocation committee exercise

The OPTICON part on proposal writing and evaluation started on Sunday 23 June. In the first part, an introductory lecture on the work of time allocation committee was presented by J. Fynbo. After the introductory lecture, logistical details for the exercise were explained however, the main idea of the exercise was very clear. Each group, with the same composition as for data reduction part, would act as a 'Telescope Time Allocation Committee'. They would all be given the same 10 proposals for discussion, and each panel would be chaired by the tutor from the data reduction part of the school. They would debate and rank the proposals, also attempting to provide useful feedback (just as would be expected from a real time allocation committee). All proposals were kindly provided by OPTICON with permission of their authors and they were anonymised. Furthermore, the real OPTICON time allocation committee rankings and feedback summaries were sent to the tutors on the last day, before the final discussion.

All in all, this meant that the participants had an opportunity to feel how a real time allocation panel works. In each group a responsible was assigned for each paper and this responsible was guiding the panel discussion with the guidance of the group tutor. The tutors were there to act as moderators, the main task of discussion about the proposals and preparation of the ranking was solely in hands of participants.

In the common session, all participants discussed each proposal. Each group provided their comments on the proposals and then presented their feedback to the others. After discussing each proposal, the summary of the OPTICON panel feedback was presented to participants for comparison. It was interesting to compare how each group's perception of the proposals differed. For some proposals, the opinion of various groups was very different, however, the clear conclusions of the session were:

- The best and the worst proposals were received by all groups in a similar way
- The best and the worst proposals had also very similar feedback from OPTICON time allocation committee to the feedback of our participants
- The "grey zone" in the middle often showed some fluctuations between groups, some of which might have been due to missing information about the proposers' team, and/or groups not reviewing proposals which would be a good match for their expertise
- In general, young researchers participating in summer school did a very good job consistent with the OPTICON time allocation committee (even though their individual experience with proposal writing and assessment was far more limited)

6. Closing and impact of the school

The school ended with a discussion after the proposal review exercise. In general, students and young researchers were very motivated and many of them had already some previous experience with e.g. IRAF and partly with proposal writing as they were involved in such tasks because of their supervisors. In the closing discussion, the organisational aspects such as ratio of lectures and group work were discussed. In general, participants prefer more group work over classical lectures - concluding that too many lectures would severely limit the time for project work.

As we would like to provide some guidance and inspiration for future summer school organisers, we decided to publish the results in the form of this proceedings. Furthermore, participants will acquire a feeling for the whole process from proposal writing to data reduction and subsequent publication as their project work which will be published here as well.

We would like to thank to local organizers led by J. Budaj and to all tutors and lecturers who contributed to the success of the school. As for ERASMUS+, the next school funded by the project will be held in summer 2020, while OPTICON plans three different schools for 2020. These types of schools have an important impact with many alumni going on to hold prestigious fellowships or posts in astronomy. Furthermore, many former participants later become tutors or organizers of these schools allowing for continuity and for education of young generation of astronomers. The high standard and impact of the schools is also demonstrated by the typical applications pressure factor which is usually around 2 and higher.

Finally, apart from the practical and scientific aspects of the school, there was also a great social dynamic among the participants (see group photo in Figure 1). On Tuesday 25 June, a hiking trip was organized to Skalnate Pleso Observatory and for those who wanted, a four hour hike to Hrebienok cottage. One group of eight students even made a detour to Tery cottage located quite high in the Tatra Mountains and with a gorgeous view. During the conference dinner (and the whole school, in general), young researchers interacted socially with tutors – an important experience for both sides ensuring the best possible working environment. We therefore believe that our school also had a strong social impact on students who could see that tutors and lecturers had their own similar difficulties, success stories or career steps. From the experience of organising this kind of school before, we also know that the connections forged in these schools will, in many cases, have a significant impact, leading to life-long friendships and collaborations.

Acknowledgements. The authors would like to acknowledge support from ERASMUS+ grant number 2017-1-CZ01-KA203-035562, and the European Union's Horizon 2020 research and innovation programme under grant agreement No 730890 (OPTICON) which funded the two summer schools and their participants. PK acknowledges

Figure 1. Group photo of summer school participants.

GACR grant 17-01752J. DJ acknowledges support from the State Research Agency (AEI) of the Spanish Ministry of Science, Innovation and Universities (MCIU) and the European Regional Development Fund (FEDER) under grant AYA2017-83383-P. DJ also acknowledges support under grant P/308614 financed by funds transferred from the Spanish Ministry of Science, Innovation and Universities, charged to the General State Budgets and with funds transferred from the General Budgets of the Autonomous Community of the Canary Islands by the Ministry of Economy, Industry, Trade and Knowledge.

References

Whelan, D. G., Privon, G. C., Beaton, R. L., et al., The Importance of Telescope Training in Data Interpretation. 2019, *arXiv e-prints*, arXiv:1907.05889

Contrib. Astron. Obs. Skalnaté Pleso **49**, 528 – 531, (2019)

Discovery of a binary quasar at z=1.76

E. Altamura[1], S. Brennan[2], A. Leśniewska[3], V. Pintér[4], S.N. dos Reis[5,6], S. Geier[7,8,9] and J.P.U. Fynbo[10,11]

[1] *Jodrell Bank Centre for Astrophysics, Department of Physics and Astronomy, The University of Manchester, Oxford Road, Manchester M13 9PL, United Kingdom*

[2] *School of Physics, OBrien Centre for Science North, University College Dublin, Belfield, Dublin 4, Ireland*

[3] *Astronomical Observatory Institute, Faculty of Physics, Adam Mickiewicz University, ul. Słoneczna 36, Poznań, Poland*

[4] *Doctoral School of Sciences, The University of Craiova, Str. A. I. Cuza nr. 13, 200585 Craiova, Romania*

[5] *Departamento de Física, Faculdade de Ciências da Universidade de Lisboa, Edifício C8, Campo Grande, 1749-016 Lisboa, Portugal*

[6] *Instituto de Astrofísica e Ciências do Espaço - Observatório Astronómico de Lisboa, Tapada da Ajuda, 1349-018 Lisboa, Portugal*

[7] *Instituto de Astrofisica de Canarias, C/ Via Lactea, s/n, 38205, La Laguna, Tenerife, Spain*

[8] *Departamento de Astrofisica, Universidad de La Laguna, 38206 La Laguna, Tenerife, Spain*

[9] *Gran Telescopio Canarias (GRANTECAN), 38205 San Cristbal de La Laguna, Tenerife, Spain*

[10] *Cosmic DAWN Center NBI/DTU-Space*

[11] *Niels Bohr Institute, University of Copenhagen, Lyngbyvej 2, 2100 Copenhagen Ø, Denmark*

Received: August 1, 2019; Accepted: September 7, 2019

Abstract. We present the serendipitous discovery of a physical pair of quasars with estimated cosmological redshift $z = 1.76$. Long-slit spectroscopic observations of the candidate quasar GQ 1114+1549A were conducted with the OSIRIS instrument at the Gran Telescopio Canarias. The orientation of the slit allowed OSIRIS to also capture the spectrum of GQ 1114+1549B, an object with angular separation of $\Delta\theta = 8.76$ arcsec from GQ 1114+1549A. Spectral analysis on the Si IV and C IV, C III] emission lines confirmed the quasar nature of GQ 1114+1549A, as well as that of its newly discovered companion. The relative intensity for the emission lines and the shape of the continuum of the two objects were found to be significantly different, rendering the hypothesis of the system being a gravitationally lensed quasar highly unlikely. The projected physical distance between the two quasars was therefore estimated to be 75 kpc.

Key words: quasars: general: emission lines, spectroscopy – quasars: individual: GQ 1114+1549, binary quasar

1. Introduction

Small-scale clustering of quasars has been object of debate for at least two decades, as it provides insight into cosmological tests of the Λ-Cold Dark Matter model and enhanced astrophysical activity of individual pairs of objects (see e.g. Mortlock et al., 1999; Sergeyev et al., 2016; Shalyapin et al., 2018, and references therein). In this project we analysed optical spectra of quasar candidates, selected based on photometry from a range of public surveys as well as astrometric information from Gaia following the prescription of Heintz et al. (2018); Geier et al. (2019). In synergy with the SDSS photometric selection, the Gaia-assisted method was able to reliably identify extra-galactic sources from their parallax consistent with zero (Geier et al., 2019). Such selection, presented by Geier et al. (2019), resulted in a catalogue of candidate quasars, which were then spectroscopically observed, in order to confirm or confute their extra-galactic nature. GQ 1114+1549 was included in the catalogue constructed by (Geier et al., 2019) and its quasar nature spectroscopically confirmed.

In the present work, we analysed the spectral data relative to GQ 1114+1549 and found evidence of a second unknown quasar, GQ 1114+1549B, separated by 8.76 arcsec from its companion. The determination of systemic redshifts, as well as emission and broad absorption lines, indicate that GQ 1114+1549 is highly likely to be a gravitationally bound quasar pair, which is the object of our study.

2. Observations and results

The primary quasar has equatorial coordinates $RA = 168.6417$ deg, $Dec = +15.8292$ deg (J2000.0) (see also Heintz et al., 2018; Geier et al., 2019) and it is hereafter identified as GQ 1114+1549A. The spectra used in the project originate from a project (PI S. Geier) running at the Gran Telescopio Canarias (GTC), which allowed the observation of GQ 1114+1549A on December 4, 2018, when two exposures with 400 second integration time were secured. The Grism 1000B, combined with a 1.23 arcsec slit, provided a resolution of $\mathcal{R} = 500$ and a spectral range of 3750–7800 Å. The atmospheric conditions presented a seeing of 1.2 arcsec, which allowed the observation of the target at an air mass of 1.46 using a parallactic slit angle.

Alongside with the spectrum of GQ 1114+1549A, two other objects were covered by the slit, as shown in the top panel of Figure 1. The unidentified faint source located above the main target in the slit was found to display the broad emission lines typical of quasars. Due to the low signal-to-noise ratio for this source, the spectrum is plotted using a larger bin size, in order to enhance the visibility of the emission lines. In the two bottom panels of figure 1 we show the 1-dimensional spectra of the main target GQ 1114+1549A and its weaker companion, which we henceforth refer to as GQ 1114+1549B. The redshift for both objects, $z = 1.76$, was computed based on the presence of emission lines from Si IV and C IV, and C III].

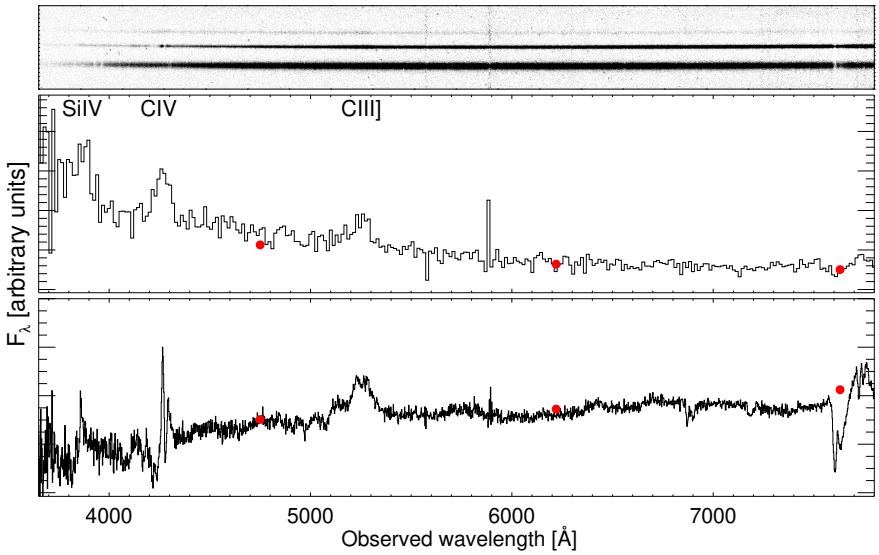

Figure 1. This figure presents the GTC spectra, where the Si IV and C IV, C III] lines are indicated. The top panel shows the section of a 2-dimensional spectra with three objects on the slit. The bottom trace is a star, the central trace is the primary target and the upper trace is the serendipitously discovered quasar. The two bottom panels display the 1-dimensional quasar spectra of GQ 1114+1549A (below) and B (above). Due to a misalignment between the B-object and the slit, the flux of the B-spectrum was suppressed by a factor of ~ 10 and was therefore binned by a factor of seven for better visibility. The red circles represent the g, r, and i-band photometry from the SDSS (York et al., 2000), which sets the scale for the photometric information.

3. Discussion and conclusion

By using images from the Sloan Digital Sky Survey (SDSS; York et al., 2000), centred on GQ 1114+1549A, we have inferred that GQ 1114+1549 A and B appear as two point sources separated by 8.76 arcsec. The slit orientation only marginally covers the position of GQ 1114+1549B, which explains the low signal-to-noise ratio for the GQ 1114+1549B spectrum. However, both the GTC spectra and the SDSS photometry allowed to identify significant differences in spectral shapes between the two objects. In particular, GQ 1114+1549A is a reddened source with strong associated absorption lines, whereas GQ 1114+1549B appears to be a blue quasar. The pair is therefore highly unlikely to arise from a gravitationally lensed quasar and the projected physical separation between GQ 1114+1549 A and B was hence found to be 75 kpc.

Further observations and analyses of this quasar pair will be presented in an upcoming paper.

Acknowledgements. We thank the organisers of the OPTION/ERASMUS+ summer school and the staff at Skalnaté Pleso Observatory for a very constructive experience in the high Tatras region. The purpose of the summer school, which took place in June 2019, was to discuss the process of developing scientific proposals for observing time, reducing data, performing analyses and ultimately elaborating publications.

References

Geier, S. J., Heintz, K. E., Fynbo, J. P. U., et al., Gaia-assisted selection of a quasar reddened by dust in an extremely strong damped Lyman-α absorber at z = 2.226. 2019, *Astron. Astrophys.*, **625**, L9, DOI: 10.1051/0004-6361/201935108

Heintz, K. E., Fynbo, J. P. U., Høg, E., et al., Unidentified quasars among stationary objects from Gaia DR2. 2018, *Astron. Astrophys.*, **615**, L8, DOI: 10.1051/0004-6361/201833396

Mortlock, D. J., Webster, R. L., & Francis, P. J., Binary quasars. 1999, *Mon. Not. R. Astron. Soc.*, **309**, 836, DOI: 10.1046/j.1365-8711.1999.02872.x

Sergeyev, A. V., Zheleznyak, A. P., Shalyapin, V. N., & Goicoechea, L. J., Discovery of the optically bright, wide separation double quasar SDSS J1442+4055. 2016, *Mon. Not. R. Astron. Soc.*, **456**, 1948, DOI: 10.1093/mnras/stv2763

Shalyapin, V. N., Sergeyev, A. V., Goicoechea, L. J., & Zheleznyak, A. P., Spectroscopic follow-up of double quasar candidates. 2018, *Mon. Not. R. Astron. Soc.*, **480**, 2853, DOI: 10.1093/mnras/sty2028

York, D. G., Adelman, J., Anderson, Jr., J. E., et al., The Sloan Digital Sky Survey: Technical Summary. 2000, *Astron. J.*, **120**, 1579, DOI: 10.1086/301513

Contrib. Astron. Obs. Skalnaté Pleso **49**, 532 – 538, (2019)

Optical spectra of near-Earth asteroids (381906) 2010 CL19 and (453778) 2011 JK

H. Kučáková[1], O. Mikhalchenko[2], M. Popescu[3], C. Ransome[4] and A. Sharma[5]

[1] *Astronomical Institute, Academy of Sciences of the Czech Republic, Fričova 298, CZ-25165 Ondřejov, Czech Republic*

[2] *Department of Astronomy and Space Informatics, V.N. Karazin Kharkiv National University, 4 Svobody Sq., Kharkiv 61022, Ukraine*

[3] *Instituto de Astrofísica de Canarias (IAC), C/Vía Láctea s/n, 38205 La Laguna, Tenerife, Spain (E-mail: mpopescu@iac.es – corresponding author)*

[4] *Astrophysics Research Institute, Liverpool John Moores University, 146 Brownlow Hill, Liverpool L3 5RF, UK*

[5] *Istituto Nazionale di Fisica Nucleare, Sezione di Pisa, Italy*

Received: August 9, 2019; Accepted: September 26, 2019

Abstract. In the framework of the *Observational Astrophysics: from proposals to publication program* (which is an OPTICON and ERASMUS+ school), we report the spectral characterization of two near-Earth asteroids, namely (381906) 2010 CL19 and (453778) 2011 JK. The data were obtained with the 2.56 m Nordic Optical Telescope equipped with ALFOSC instrument. The spectral data reduction and the methods for analyzing the results are shown in detail. We found that (381906) 2010 CL19 is a K-type asteroid, and (453778) 2011 JK is an Sq type asteroid. The comparison with laboratory spectra of meteorites revealed spectral similarities with ordinary chondrites for both objects. Considering the average albedo corresponding to the assigned types, we estimated the size of (381906) 2010 CL19 to be in the order of 1 km, and the size of (453778) 2011 JK to be about 550 m.

Key words: minor planets; techniques: spectroscopic; methods: observations

1. Introduction

The spectral signature of asteroids is determined by the properties of their surface. In the optical and near-infrared wavelength region, the radiation that comes from these bodies corresponds mostly to the reflected Sun light. The reflectance spectra obtained from ground based observatories can be used to determine the compositional information. This is usually done by comparing the telescopic measurements with the laboratory data of meteorites and of various kind of minerals. The spectral features are explained by crystal field theory (Burns, 1993).

All authors contributed equally to the work

The reasons that motive the studies of the small celestial bodies cover both practical and scientific aspects. The asteroids are fragments of the planetesimals that once formed the planets. Because most of them didn't suffer significant geological transformations they are the pieces of the puzzle for understanding the formation and evolution of the Solar System. On the other hand, the practical reasons are the exploitation of small bodies for the space exploration and for planetary defense (e.g. Binzel et al., 2015).

Table 1. Known properties of the observed asteroids. The Δv budget (the total change in velocity required for a space mission), the Tisserand parameter (T_J) with respect to Jupiter, the absolute magnitude (H), the Minimum Orbit Intersection Distance with Earth - MOID, the rotation period - P_{syn}, and the maximum lightcurve amplitude - A_{max} (mag) are shown. The data was obtained from the JPL Small-Body Database, the Minor Planet Ceneter, Warner (2014), and Warner et al. (2009).

Target	Orbit	Δv	T_J	MOID	H	P_{syn}	A_{max}
		km/s		AU	mag	hrs	mag
381906	Apollo	8.389	4.198	0.0115306	17.8	3.5197±0.0005	0.39±0.03
453778	Amor	5.802	3.790	0.0247028	18.5	≈2.5	< 0.37

The aim of our article is to outline the methods for obtaining and analyzing optical spectral data of minor planets. To exemplify these, we present new spectra for two near-Earth asteroids, namely (381906) 2010 CL19 and (453778) 2011 JK. These were selected due to their proximity to Earth orbit, thus in the future they can be space-mission targets. Furthermore, they are catalogued as potentially hazardous asteroids, which means that on a long time scale they may pose a threat to Earth. Some of the known properties of these bodies are shown in Table 1.

Based on the albedo value, $p_V = 0.451 \pm 0.224$, obtained by NEOWISE (Nugent et al., 2016), the diameter of (381906) 2010 CL19 can be estimated to be 0.520 ± 0.111 km. The size of (453778) 2011 JK can be approximated only based on the absolute magnitude and it can range between 0.4 - 1.4 km depending on its albedo. The correlation between albedo and the spectral type allowed us to constrain significantly the dimensions of these objects.

The article is organized as follows: the Section 2 describes the observations and the steps performed for the data reduction. The obtained spectra are analyzed in Section 3. Section 4 discuss the results and summarize the paper.

2. The observing procedure and data reduction

The observations were performed using the 2.56 m Nordic Optical Telescope, located at El Roque de los Muchachos Observatory in La Palma, Canary Islands.

The instrument was the Alhambra Faint Object Spectrograph and Camera (ALFOSC). Low resolution spectroscopy is sufficient to characterize the asteroids because they show spectral bands (as they are solid bodies). Thus, the Grism_#4 was used in conjunction with a slit having a width of 1.8 arcsec. The second order blocking filter GG475 was used to avoid contamination. This setup allows us to cover the optical interval 0.48 - 0.92 μm with a resolution of $\sim$ 300.

Table 2. Log of of observations for the night of 2019 April, 24. The designation of the targets, the observation time (UT_{start}), the total exposure time, the apparent magnitude (V_{mag}) and the airmass are shown.

Target	UT_{start}	Exp. time	V_{mag}	Airmass
	$hh:mm$	*sec.*	*mag*	
SA98-978	20:43	3x15	10.6	1.548
381906	21:28	3x600	17.5	1.346
SA102-1081	22:16	3x15	9.9	1.146
453778	22:25	3x600	17.7	1.295

The observing log is shown in Table 2. Calibration images were obtained at the beginning of the night. These include biases, internal flats, and lamp (with He, Ne, ArTh) exposures for wavelength calibration. The well known solar analogues from Landolt catalogue, SA102-1081 and SA102-1081 were observed for calibrating the observed asteroids spectra.

The raw data from the telescope need to be prepared and calibrated for subsequent spectrum extraction. The preliminary step for data reduction implies the inspection of the image headers and generation of a log. The log contains the essential information about each image including the type of file (flats, biases, source spectra etc.), the coordinates, the exposure time, the instrument information, and the atmospheric conditions at the time and of the data acquisition.

The preparation of the images include the trimming of the over-scan and non-target regions. The next step is to combine an average of the bias frames which show the digital readout flaws, using standard routines in `IRAF`. The raw images are then de-biased using the final master bias. In much the same way we produce a master flat which corrects for flaws in the optical instrumentation. All these tasks are automatized using additional `python` scripts.

The extraction of the asteroid spectra is achieved with the help of the *apall* package, available through `IRAF` software (*noao* $\rightarrow$ *onedspec* $\rightarrow$ *apextract*). The *apall* package combines all the spectrum extraction utilities into one and is a handy tool for simple spectrum extraction. The outline of the extraction procedure using this package is the following: 1) find the spectrum on the CCD image; 2) define the extraction and background windows in pixels; 3) trace the center of spatial profile along the dispersion axis; 4) sum the spectrum within

the extraction window, subtracting sky background at each step. At this step, the extracted spectrum is in units of signal (ADU - Analog to Digital Unit) per pixel of the CCD. The Ox-axis is represented by the pixel number. We used `IRAF` again and lamp flats to fit our wavelength to known emission lines from the Calibration lamps.

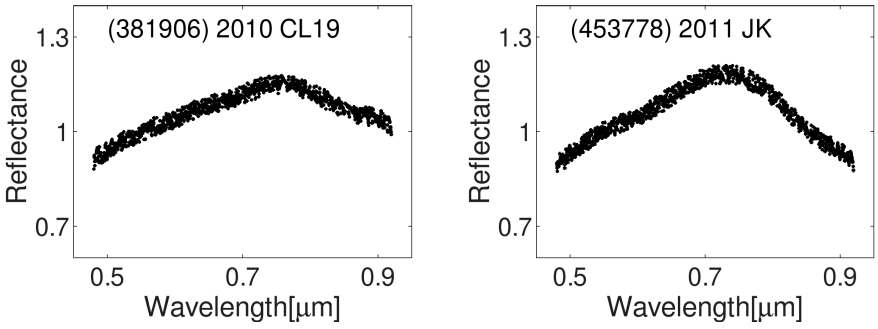

Figure 1. The optical reflectance spectra of the NEAs studied in this work. The spectra were normalized to be 1 at 0.55 μm.

The final step is to obtain the reflectance spectrum. This is done by dividing the observed asteroid spectrum with the spectra of the two solar analogue stars. Both solar analogues give similar results in terms of spectral shape. This validates the observations and the data reduction process (we note that both stars are well known solar analogues used for calibrating asteroid reflectance spectra). The final reflectance spectra, shown in Fig. 1, are obtained relative to SA102-1081. This has been selected because is closer in terms of airmass.

3. Results

The spectra we obtained are analyzed to determine their taxonomic classification and compared to the spectra of meteorites obtained in laboratory. Considering the correlation between the spectral classes and albedo we can compute the diameter of the asteroids.

The taxonomic classification provides a general characterization of asteroid spectra and a common language for their comparison. Among the most used taxonomies is the one of Bus & Binzel (2002), which covers optical wavelengths. The updated version proposed by DeMeo et al. (2009) covers the entire 0.45 - 2.45 μm interval. To classify our spectra we used a χ^2 minimization between the various spectral templates of DeMeo et al. (2009) and our observed asteroid reflectances. We found that (381906) 2010 CL19 belongs to the K-type asteroid class and (453778) 2011 JK is an Sq-type. These results are shown in Fig. 2.

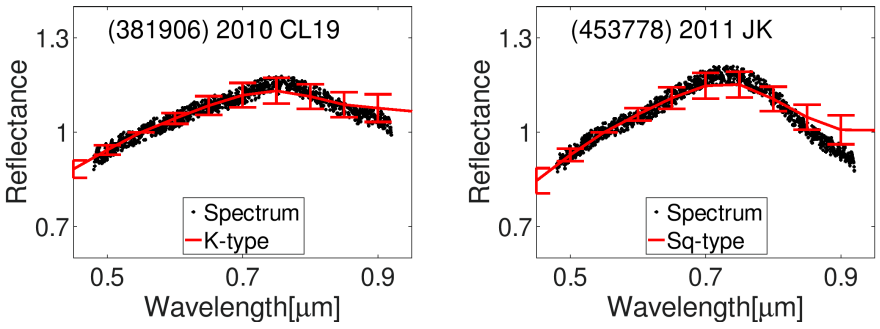

Figure 2. Comparison between the observed asteroid spectra and the assigned taxonomic classes.

Besides sorting our asteroids into classes according to DeMeo et al. (2009) taxonomic scheme, we can also use our spectra to determine what meteorite sample found on Earth resembles the asteroid the closest. This connects the laboratory data with the spectral properties of celestial objects providing the basis for interpreting the composition of these small bodies of the Solar System. This algorithm was implemented in `python` and it applies χ^2 test to find the meteorite spectrum from the Relab database that best fits our data.

We found that (381906) 2010 CL19 shows similarities with ordinary chondrite meteorites. However, the spectrum that best matched it corresponds to a sample of Divnoe meteorite (Sample ID: MB-CMP-015-L), which is categorized as a primitive achondrite. This ambiguity is due to the fact that the presence of 0.9 μm band is not sufficient to distinguish between various olivine-pyroxene compositions.

The spectral curve of (453778) 2011 JK is matched by several ordinary chondrite meteorites. The best fit corresponds to a sample from Knyahina meteorite (Sample ID: MR-MJG-049), which is an L5 ordinary chondrite.

We note that these results give an indication to certain types of compositions, but the solution is not unique and observations in other wavelength regions can improve it. Mineralogical models can be applied for spectra covering the optical to near-infrared interval.

4. Discussions and conclusions

The results of Mainzer et al. (2011) show a direct relation between the spectral type and the albedo. They provide the average value of visual geometric albedo p_V for each taxonomic class defined by DeMeo et al. (2009). Furthermore, the geometric albedo p_V, the absolute magnitude H, and the diameter

D are associated by the well-known formula (e.g. Harris & Lagerros, 2002): $D = 1329 \times 10^{-0.2H}/\sqrt{p_V}$.

We classified (453778) 2011 JK as Sq type. Therefore, using the absolute magnitudes H (shown in Table 1) and the average S-class value of the albedo $p_V = 0.23 \pm 0.02$ we can estimate for the first time the diameter for (453778) 2011 JK as $D \approx 550m$. The K-type assigned to the asteroid (381906) 2010 CL19, has an associated albedo ($p_V = 0.13 \pm 0.058$). Based on this value we can estimate its size to 1 km. This value is significantly larger compared to the one estimated based on the measured albedo, $p_V = 0.451 \pm 0.224$ (Nugent et al., 2016), which gives about 0.55 km.

The fact that the spectrum of (453778) 2011 JK is very similar to the spectra of the ordinary chondrites suggests that it may be the remnant of a much more primitive, and therefore, an ancient object of the Solar System.

Complementary observations using various techniques (polarimetry, near-infrared spectra, radar) can further constrain the physical and the dynamical properties of these asteroids. Altogether, these will allow to trace and predict the evolutionary path of these celestial bodies.

Acknowledgements. The authors would like to acknowledge support from ERASMUS+ grant number 2017-1-CZ01-KA203-035562, and the European Union's Horizon 2020 research and innovation programme under grant agreement No 730890 (OPTICON). The asteroid spectra were obtained in the framework of e P3NEOI project financed by ESA.

The following databases and web-resources were used in this work: JPL Small-Body Database[1], IAU Minor Planet Center[2], NEA Delta-V for Spacecraft Rendezvous[3], Relab database[4], Asteroid Lightcurve Photometry Database-ALCDEF[5].

References

Binzel, R. P., Reddy, V., & Dunn, T. L. 2015, *The Near-Earth Object Population: Connections to Comets, Main-Belt Asteroids, and Meteorites; in Asteroids IV*, ed. P. Michel, F. E. DeMeo, & W. F. Bottke (Tucson: University of Arizona Press), 243–256

Burns, R. G. 1993, *Mineralogical Applications of Crystal Field Theory*, 575

Bus, S. J. & Binzel, R. P., Phase II of the Small Main-Belt Asteroid Spectroscopic Survey. A Feature-Based Taxonomy. 2002, *Icarus*, **158**, 146, DOI: 10.1006/icar.2002.6856

[1] `https://ssd.jpl.nasa.gov/sbdb.cgi`

[2] `https://minorplanetcenter.net/`

[3] `https://echo.jpl.nasa.gov/~lance/delta_v/delta_v.rendezvous.html`

[4] `http://www.planetary.brown.edu/relab/`

[5] `http://alcdef.org/`

DeMeo, F. E., Binzel, R. P., Slivan, S. M., & Bus, S. J., An extension of the Bus asteroid taxonomy into the near-infrared. 2009, *Icarus*, **202**, 160, DOI: 10.1016/j.icarus.2009.02.005

Harris, A. W. & Lagerros, J. S. V. 2002, *Asteroids in the Thermal Infrared; in Asteroids III*, ed. W. F. Bottke, Jr., A. Cellino, P. Paolicchi, & R. P. Binzel (Tucson: University of Arizona Press), 205–218

Mainzer, A., Grav, T., Masiero, J., et al., NEOWISE Studies of Spectrophotometrically Classified Asteroids: Preliminary Results. 2011, *Astrophys. J.*, **741**, 90, DOI: 10.1088/0004-637X/741/2/90

Nugent, C. R., Mainzer, A., Bauer, J., et al., NEOWISE Reactivation Mission Year Two: Asteroid Diameters and Albedos. 2016, *Astron. J.*, **152**, 63, DOI: 10.3847/0004-6256/152/3/63

Warner, B. D., Near-Earth Asteroid Lightcurve Analysis at CS3-Palmer Divide Station: 2013 September-December. 2014, *Minor Planet Bulletin*, **41**, 113

Warner, B. D., Harris, A. W., & Pravec, P., The asteroid lightcurve database. 2009, *Icarus*, **202**, 134, DOI: 10.1016/j.icarus.2009.02.003

Contrib. Astron. Obs. Skalnaté Pleso **49**, 539 – 545, (2019)

Quest to find Changing Look-Quasars

T. Pursimo[1], L. Ighina[2,3], N. Ihanec[4], N. Mandarakas[5,6], K. Skillen[7] and S. Terefe[8]

[1] *Nordic Optical Telescope, Apartado 474, E-38700 Santa Cruz de La Palma, Spain (E-mail: tpursimo@not.iac.es)*

[2] *Dipartimento di Fisica G. Occhialini, Università degli Studi Milano-Bicocca, Piazza della Scienza 3, I-20126 Milano, Italy*

[3] *INAF, Osservatorio Astronomico di Brera, via Brera 28, I-20121 Milano, Italy*

[4] *Warsaw University Astronomical Observatory, Al. Ujazdowskie 4, 00-478 Warsaw, Poland*

[5] *Department of Physics, University of Crete, GR-71003, Heraklion, Greece*

[6] *Foundation for Research and Technology - Hellas, IESL & Institute of Astrophysics, Voutes, 7110 Heraklion, Greece*

[7] *School of Physics, Trinity College Dublin, The University of Dublin, Dublin 2, Ireland*

[8] *Ethiopian Space Science and Technology Institute, Department of Astronomy and Astrophysics*

Received: July 31, 2019; Accepted: September 25, 2019

Abstract. We present the optical analysis of a sample of quasars selected for their significant variation in optical emission. Photometric analysis was carried for 22 sources and it was found that the colour change for the majority of the sample follows a typical behavior of Changing Look Quasars (CLQs) as suggested in the literature. Spectroscopic analysis was carried out on 2 sources to identify the origin of the observed variation.

Key words: galaxy:active – quasars: emission lines – quasars: general

1. Introduction

Optical properties of Quasi-Stellar Objects (QSOs) have been well characterized in the past decade thanks to large-scale surveys such as the Sloan Digital Sky Survey (SDSS, Vanden Berk et al. 2004) and, more recently, Pan-STARRS1 (PS1, Simm et al. 2015). Observations from different surveys show the typical variation of the optical continuum of QSOs is of the order of ~ 0.2 mag, ranging in timescales from several months to years (e.g. MacLeod et al. 2012). These changes in the optical emission are usually associated with instabilities and inhomogeneities of the accretion disk (e.g. Kokubo 2015). Their spectral features, especially the Broad Emission Lines (BELs), however, are generally more stable and lagged with respect to the continuum (e.g. Shen et al. 2015).

Yet, a few exceptions of quasars with very large variability in the optical continuum (~ 1 mag) have been discovered with the concurrent emergence or disappearance of BELs (e.g. Denney et al. 2014). In some of these sources, the variations are on timescales of a few months and can be related to Tidal Disruption Events (e.g. Gezari et al. 2015), slow Microlensing Outbursts (e.g. Bruce et al. 2017) or, in the case of Blazars, to the presence of a jet (e.g. Marscher et al. 2008). The most challenging to explain are the Changing Look Quasars (CLQs) (MacLeod et al. 2016), where the large spectral variability is on the timescale of years (e.g. LaMassa et al. 2015). The number of known sources of this kind is very limited, but in recent years, all-sky space surveys such as Gaia (Gaia Collaboration et al., 2016) present a remarkable opportunity to increase the size of this population. With a sufficiently large sample of CLQs, it will be possible to revise current models of the accretion disk and the Broad Line Region (BLR) structures in Active Galactic Nuclei (AGNs) to account for this new class of sources.

2. Observations and data reduction

Half of the targets used in this project were selected from ESA's highly precise astrometic mission Gaia, which scans the whole sky and can detect variability in magnitude with precision of 0.001, down to 20 mag. In particular, they were chosen from Gaia Science Alerts program[1], which searches for transient phenomena that show sudden changes in magnitude and thus is ideal for the discovery of CLQs. The other half of the sample was selected by comparing Gaia and SDSS DR 12 data (Kostrzewa-Rutkowska et al. 2018).
To fully classify these transients, photometric and spectroscopic follow-up observations were carried out at the Nordic Optical Telescope (NOT, La Palma, Spain). Photometric data were obtained for 22 targets using the Alhambra Faint Object Spectrograph and Camera (ALFOSC) on NOT in the SDSS g, r and i band filters. We obtained low resolution spectrum for two objects using ALFOSC, the same night as the photometric data, with the spectral range of 3200-9200Å at a resolution of R=330. The data were processed using the standard IRAF reduction and calibration. The apparent magnitudes of the targets were deduced with aperture photometry, using archival SDSS data for magnitudes of comparison stars.

3. Results and Discussion

3.1. Photometry

The results of the photometric analysis are presented in appendix A together with comparison archival data from SDSS. Figure 1 shows the variation of g-

[1]http://gsaweb.ast.cam.ac.uk/alerts/

r (new - historic) colour as a function of the difference between the new and historic magnitudes in the g band. Most of the sources seem to follow the known

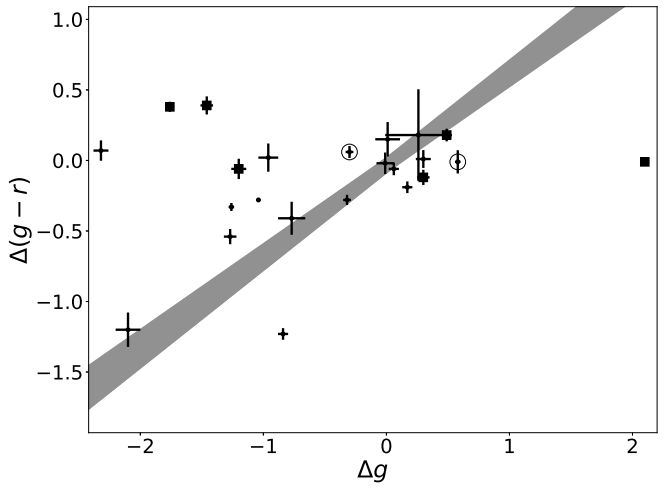

Figure 1. Variation of the g-r colour (new - historic) as a function of magnitude variability g-g_{SDSS}. The shaded region represents the observational relation (with its 1σ uncertainty) found in Yang et al. (2018) for CLQs. The few QSOs detected also in the radio band are depicted with squares, while the sources whose spectrum is discussed in this work have been highlighted with a circle.

trend for confirmed CLQs ("bluer-when-brighter") found by Yang et al. 2018 using a sample of 21 CLQs. However, there are a few objects, among which most of the radio detected ones (reported as squares), that do not follow a clear pattern. It is probable that in these cases the change in magnitude is caused by external (to the AGN structure) events, such as the ones mentioned in Section 1.

3.2. Spectroscopy

We performed spectroscopic analysis for two targets; Gaia19bwn and Gaia18dsk. Figure 2 shows the comparison between the observed spectra and archival SDSS spectra (right panel), together with their respective light curves (left column). The Gaia19bwn spectrum (Figure 2, top panel) is dominated by strong, slightly broadened Balmer lines, visible down to Hη (3866 Å). The archival SDSS spectrum has strong Hα and the Hβ and forbidden [OIII] lines (4862 Å and 5008

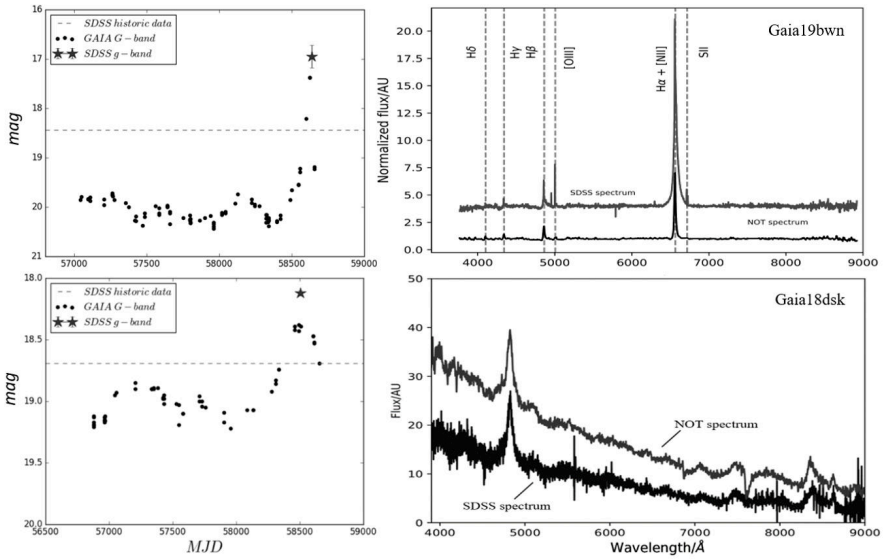

Figure 2. Light curves (left) and optical spectra (right) for Gaia19bwn (top) and Gaia18dsk (bottom). The Gaia19bwn spectra have been normalized and the SDSS spectrum has an offset for clarity

Å respectively) have similar fluxes, but the new NOT spectrum shows weaker Hα and the Hβ flux is now four times stronger then the [OIII]. We estimate the redshift based on Balmer lines to z=0.009, which is consistent with the SDSS archival value. The spectrum displays brightening in the continuum and its BELs, as well as some narrow emission features, typically not found in the quasar spectra. Interestingly, using GELATO[2], we classified Gaia19bwn as a Type II supernova, with a 92% confidence level (Pursimo et al., 2019), however the SDSS classification is broad line AGN.

In the case of Gaia19dsk (Figure 2, bottom panel), the variation in magnitude was related to an increase of the overall optical continuum. Though the NOT observation was carried out during the peak of the light curve, the spectral features of the source remained unchanged, suggesting that the structure of the BLR did not vary during this event.

Acknowledgements. We are very thankful to H. Korhonen and to all the team for organizing the summer school *Observational astrophysics: from proposal to publication*. The authors would also like to acknowledge support from ERASMUS+ grant number 2017-1-CZ01-KA203-035562, and the European Union's Horizon 2020 research and innovation programme under grant agreement No 730890 (OPTICON). This work has

[2]https://gelato.tng.iac.es/

made use of data from the European Space Agency (ESA) mission *Gaia*, processed by the *Gaia* Data Processing and Analysis Consortium (DPAC) and the Photometric Science Alerts Team. Funding for the DPAC has been provided by national institutions, in particular the institutions participating in the *Gaia* Multilateral Agreement. In this work we also made use of SDSS data. Funding for the Sloan Digital Sky Survey IV has been provided by the Alfred P. Sloan Foundation, the U.S. Department of Energy Office of Science, and the Participating Institutions. SDSS acknowledges support and resources from the Center for High-Performance Computing at the University of Utah. The data presented here were obtained with ALFOSC, which is provided by the Instituto de Astrofisica de Andalucia (IAA) under a joint agreement with the University of Copenhagen and NOTSA.

References

Becker, R. H., White, R. L., & Helfand, D. J., The FIRST Survey: Faint Images of the Radio Sky at Twenty Centimeters. 1995, *Astrophys. J.*, **450**, 559, DOI: 10.1086/176166

Bruce, A., Lawrence, A., MacLeod, C., et al., Spectral analysis of four 'hypervariable' AGN: a micro-needle in the haystack? 2017, *Mon. Not. R. Astron. Soc.*, **467**, 1259

Condon, J. J., Cotton, W. D., Greisen, E. W., et al., The NRAO VLA Sky Survey. 1998, *Astron. J.*, **115**, 1693, DOI: 10.1086/300337

Denney, K. D., De Rosa, G., Croxall, K., et al., The Typecasting of Active Galactic Nuclei: Mrk 590 no Longer Fits the Role. 2014, *Astrophys. J.*, **796**, 134, DOI: 10.1088/0004-637X/796/2/134

Gaia Collaboration, Prusti, T., de Bruijne, J. H. J., et al., The Gaia mission. 2016, *Astron. Astrophys.*, **595**, A1

Gezari, S., Chornock, R., Lawrence, A., et al., PS1-10jh Continues to Follow the Fallback Accretion Rate of a Tidally Disrupted Star. 2015, *Astrophys. J., Lett.*, **815**, L5

Kokubo, M., Constraints on the temperature inhomogeneity in quasar accretion discs from the ultraviolet-optical spectral variability. 2015, *Mon. Not. R. Astron. Soc.*, **449**, 94

Kostrzewa-Rutkowska, Z.and Jonker, P. G., Hodgkin, S. T., Wyrzykowski, ., et al., Gaia transients in galactic nuclei. 2018, *MNRAS*, **481**

LaMassa, S. M., Cales, S., Moran, E. C., et al., The Discovery of the First "Changing Look" Quasar: New Insights Into the Physics and Phenomenology of Active Galactic Nucleus. 2015, *Astrophys. J.*, **800**, 144

MacLeod, C. L., Ivezić, Ž., Sesar, B., et al., A Description of Quasar Variability Measured Using Repeated SDSS and POSS Imaging. 2012, *Astrophys. J.*, **753**, 106, DOI: 10.1088/0004-637X/753/2/106

MacLeod, C. L., Ross, N. P., Lawrence, A., et al., A systematic search for changing-look quasars in SDSS. 2016, *Mon. Not. R. Astron. Soc.*, **457**, 389

Marscher, A. P., Jorstad, S. G., D'Arcangelo, F. D., et al., The inner jet of an active galactic nucleus as revealed by a radio-to-γ-ray outburst. 2008, *Nature*, **452**, 966

Pursimo, T., Galindo-Guil, F., Dennefeld, M., et al., Spectroscopic follow-up of transient Gaia19bwn. 2019, *The Astronomer's Telegram*, **12911**

Shen, Y., Brandt, W. N., Dawson, K. S., et al., The Sloan Digital Sky Survey Reverberation Mapping Project: Technical Overview. 2015, *Astrophys. J., Suppl.*, **216**, 4

Simm, T., Saglia, R., Salvato, M., et al., Pan-STARRS1 variability of XMM-COSMOS AGN. I. Impact on photometric redshifts. 2015, *Astron. Astrophys.*, **584**, A106

Vanden Berk, D. E., Wilhite, B. C., Kron, R. G., et al., The Ensemble Photometric Variability of ~25,000 Quasars in the Sloan Digital Sky Survey. 2004, *Astrophys. J.*, **601**, 692

Yang, Q., Wu, X.-B., Fan, X., et al., Discovery of 21 New Changing-look AGNs in the Northern Sky. 2018, *Astrophys. J.*, **862**, 109, DOI: 10.3847/1538-4357/aaca3a

A. Photometric data

In this appendix, the full data set calculated in the photometric analysis of this investigation is presented.

Table 1. Apparent magnitudes and errors of our targets in SDSS *g,r* filters along with archival magnitude from SDSS. We also report the sky coordinates of the sources (RA, DEC expressed in degrees), if the target has been detected either NVSS (The NRAO VLA Sky Survey, Condon et al. 1998) or FIRST (Faint Images of the Radio Sky at Twenty-cm, Becker et al. 1995) surveys and the date of the observation with NOT.

Object	RA	DEC	Date	Radio	g-mag ± er.	SDSS-g	Δg (NOT-SDSS)	r-mag ± er.	SDSS-r
Gaia18dry_1	215.62654	32.38623	2019-01-25	NVSS	17.32 (0.03)	19.08	-1.76	17.01 (0.02)	19.15
Gaia18dry_2			2019-01-26	NVSS	17.62 (0.05)	19.08	-1.46	17.30 (0.04)	19.15
Gaia18dsk	191.86398	22.55420	2019-01-21		18.39 (0.03)	18.69	-0.30	18.41 (0.03)	18.77
Gaia18dtm	218.84144	20.35494	2019-01-26	NVSS	18.00 (0.06)	19.20	-1.20	17.64 (0.04)	18.78
Gaia18due	359.99444	-1.20707	2019-01-24		18.70 (0.01)	18.69	0.01	18.54 (0.07)	18.68
Gaia19abd	218.83473	1.21172	2019-01-24		19.23 (0.18)	20.12	-0.89	18.98 (0.11)	20.03
Gaia19aul	133.69072	46.10460	2019-03-16		18.20 (0.10)	20.30	-2.10	18.92 (0.07)	19.82
Gaia19auy	250.74506	39.81031	2019-04-16	NVSS	17.79 (0.02)	15.69	2.10	17.50 (0.02)	15.39
Gaia19axp	216.94333	29.51063	2019-03-16		18.64 (0.01)	19.68	-1.04	18.39 (0.01)	19.15
Gaia19bbw	232.42584	35.14759	2019-04-16		17.30 (0.02)	18.56	-1.26	17.13 (0.02)	18.06
Gaia19buq	124.36008	10.20280	2019-05-28		16.47 (0.06)	18.79	-2.32	15.85 (0.04)	18.24
Gaia19bwn	173.34991	55.07108	2019-06-05		16.95 (0.02)	16.37	0.58	16.80 (0.08)	16.21
GNTJ015804-00522	29.51981	-0.872742	2019-01-23		17.35 (0.05)	18.62	-1.27	17.35 (0.02)	18.08
GNTJ025514-040655	43.809466	-4.11552	2019-01-23		18.43 (0.11)	19.20	-0.77	18.05 (0.04)	18.41
GNTJ080115+110156	120.31654	11.03237	2019-01-26		17.38 (0.27)	17.12	0.26	16.36 (0.18)	16.28
GNTJ081152+252521	122.96712	25.42259	2019-01-25		19.01 (0.03)	19.33	-0.32	18.32 (0.02)	18.36
GNTJ085554+005111	133.97614	0.85306	2019-01-26	FIRST	16.95 (0.05)	16.65	0.30	16.37 (0.02)	15.95
GNTJ130638+072124	196.66031	7.35670	2019-03-16		17.31 (0.07)	17.35	-0.04	16.90 (0.03)	16.89
GNTJ131428+054307	198.61703	5.71869	2019-03-16		17.31 (0.04)	18.18	-0.87	17.98 (0.01)	17.59
GNTJ131839+463016	199.66412	46.50460	2019-05-29		17.86 (0.04)	17.80	0.06	17.33 (0.02)	17.21
GNTJ150906+611640	227.27625	61.27780	2019-04-16		16.76 (0.04)	16.59	0.17	16.33 (0.01)	15.97
GNTJ155513+564416	238.80611	56.73792	2019-05-29	FIRST	19.28 (0.04)	18.79	0.49	18.42 (0.02)	18.11
GNTJ171955+414049	259.98271	41.68040	2019-04-16		18.36 (0.06)	18.06	0.30	17.84 (0.02)	17.55

Contrib. Astron. Obs. Skalnaté Pleso **49**, 546 – 550, (2019)

Independent study and spectral classification of a sample of poorly studied high proper motion M-dwarf candidate stars

C. Cabello[1], G. Csörnyei[2,3], J. Merc[4,5], V. Ferreirós Lopez[6] and P. Pessev[7,8,9]

[1] *Departamento de Física de la Tierra y Astrofísica. Instituto de Física de Partículas y del Cosmos (IPARCOS), Universidad Complutense de Madrid, E-28040 Madrid, Spain, (E-mail: criscabe@ucm.es)*

[2] *Institute of Physics, Eötvös Loránd University, Pázmány Péter sétány 1/a, 1117 Budapest, Hungary, (E-mail: csornyei.geza@csfk.mta.hu)*

[3] *Konkoly Observatory, Research Centre for Astronomy and Earth Sciences, Konkoly Thege Miklós út 15-17, 1121 Budapest, Hungary*

[4] *Astronomical Institute, Faculty of Mathematics and Physics, Charles University, V Holešovičkách 2, 180 00 Prague, Czech Republic, (E-mail: jaroslav.merc@gmail.com)*

[5] *Institute of Physics, Faculty of Science, P. J. Šafárik University, Park Angelinum 9, 040 01 Košice, Slovak Republic*

[6] *Physics department, Lancaster University, LA1 4YW Lancaster, United Kingdom, (E-mail: veronica.ferreiros@gmail.com)*

[7] *Gran Telescopio Canarias (GTC), La Palma, Tenerife, Spain, (E-mail: peter.pessev@gtc.iac.es)*

[8] *Instituto de Astrofísica de Canarias (IAC), La Laguna, Tenerife, Spain*

[9] *Universidad de La Laguna, Departamento de Astrofísica, La Laguna, Tenerife, Spain*

Received: September 9, 2019; Accepted: November 14, 2019

Abstract. We report an independent spectral classification of a sample of poorly studied M-dwarf candidate stars observed with the OSIRIS instrument at GTC. Our project was carried out as an independent test of the spectral classification. It is crucial for the studies of extrasolar planets orbiting M-dwarfs, since properties of the host star are directly related to understanding the planet properties and possible habitability. Understanding of the statistical properties of the dwarf stars is also crucial for the Simple Stellar Population models that play a major role in the modern astrophysics. Hα emission was detected in 33% of the sample with evidence of Hα variability in one object.

Key words: M dwarfs – stars

1. Introduction

Late-type dwarfs are the least massive (M $\sim$ 0.08 - 0.60 M$\odot$) and coolest stars (T_{eff} $\sim$ 2300 - 3800 K) on the main sequence. They are the most populous objects in the Galaxy (up to $\sim$ 70% of all stars, Henry et al., 1997), but their observations are difficult due to their low luminosity (L $\sim$ 0.0002 - 0.08 L$\odot$). Analysis of their physical properties is essential for the characterisation of the population of low-mass stars in the Galaxy. It also has significant impact on the initial mass function (IMF), simple stellar population (SSP) and evolutionary population synthesis (ESP) models. Some red dwarfs are known hosts of extrasollar planets (also of "super-Earth" size).

These stars evolve very slowly (for trillions of years), moreover red dwarfs with the mass less than 0.35 M$\odot$ are fully convective (Reiners & Basri, 2009) therefore the produced helium is remixed with the material of the star prolonging the time they spend on the main sequence. This is the reason why late-type dwarfs have not reached advanced stages of their evolution yet.

Their spectra are dominated by the absorption molecular bands. Some of them reveal strong magnetic activity (Balmer lines, mainly Hα in emission).

2. Target selection and instrumental setup

This work is primarily based on optical spectroscopic data obtained with the OSIRIS instrument at Gran Telescopio Canarias (GTC), using Long Slit mode. The configuration was R1000R+GR, covering the wavelength range of 5100 - 10000 Å. Observations were carried out at the parallactic angle trough the 1 arcsecond long slit. The data set was obtained through a queue programme between September 2016 and January 2017 (semester 16B). The basics of the sample selection is relying on the 2MASS color indices (Metodieva et al., 2015) in order to avoid contamination by giant stars or galaxies. A limit of proper motion greater of 0.3 arcseconds/year was imposed in order to separate nearby dwarfs from more distant giants. The sample selection was carried out before GAIA DR1 and the proper motions were mostly derived from 2MASS and ALLWISE with a baseline of the observations between 9 and 13 years. Objects in the range $9 < J < 16$ were selected for the observations since brighter objects are most likely already studied and fainter ones were not suitable for observing within relatively short observing blocks even with GTC.

3. Data reduction

Each obtained spectral frame has been processed with the basic long slit spectroscopy reduction included in IRAF (Tody, 1986). By combining the individual spectra in each observing block, significant amount of the random noise introduced by the cosmic rays have been mitigated. The resulting spectra were suffi-

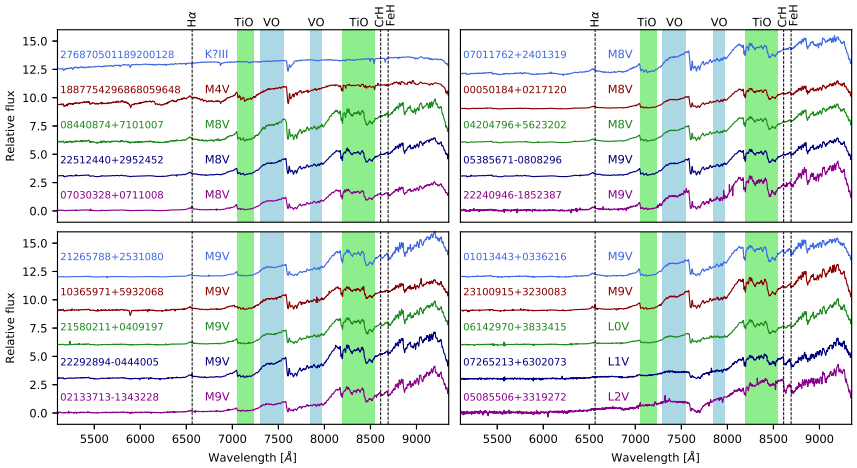

Figure 1. The extracted spectra along with the spectral types determined by `pyhammer` and their identifiers from 2MASS. For those two objects, which had no 2MASS identifier (top left panel) the Gaia identifier were given.

cient for the type determination, which has been performed with the `pyhammer python` package (Kesseli et al., 2017). This package determines the spectral type of the object by comparing various spectral templates to the input spectra, then determining the best fitting one with the help of the least square fit method.

4. Results

We have analysed a total of 20 spectra: 16 corresponds to M-dwarfs, from types M4 to M9, 3 are classified as early types of L-dwarfs (L0-L2). The object Gaia DR2 276870501189200128 is a K giant star. Figure 1 shows the spectra for each of our targets[1]. Oxides molecules like TiO λ7053 Å or VO λ7400 Å bands which dominate the far-optical portions of late M-spectra are replaced by metallic hybrids like FeH λ8692 Å and CrH λ8611 Å or neutral alkalis (doublets Rb I λ7800 Å λ7948 Å, Cs I λ8521 Å λ8943Å, Na I λ5889 Å λ5895 Å) as the strongest and more significant features in early L-type stars. M-dwarfs can show signals of chromospheric activity and flares. Some studies like Delfosse et al. (1998), Mohanty & Basri (2003) relate high activity with a faster rotation of the star. Schöfer et al. (2019) indicates that stronger magnetic fields in the active stars lead to Zeeman broadening of the individual lines in the band. Hα is a good indicator of chromospheric activity. According to Cram & Mullan (1979),

[1]We should note that the K giant and the M4 dwarf, were not primary targets of the observations and their spectra were recorded together with other dwarf stars only by chance.

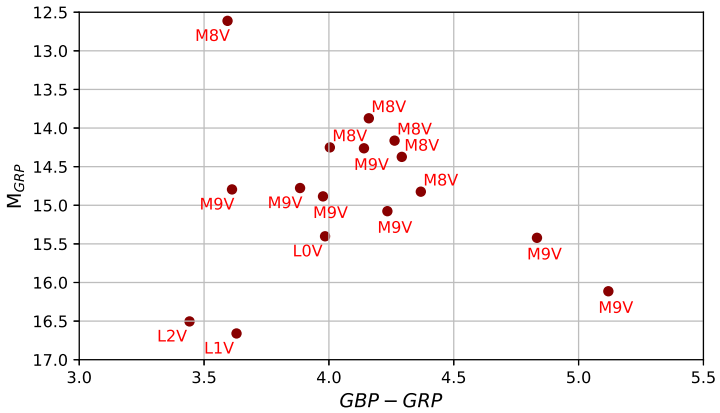

Figure 2. The Gaia color-magnitude diagram of our sample of stars. GBP and GRP stand for the blue and red Gaia bands respectively, while M_{GRP} is the absolute magnitude in the red band.

Hα goes into deeper absorption for low activity levels and into emission with increasing activity strength. Figure 1 shows Hα emission specially visible in M stars. Stars in our sample which show a strongest Hα and consequently a higher level of activity are the M4 Gaia DR2 1887754296868059648, the M8 2MASS J22512440+2952452 and M8 2MASS J08440874+7101007.

We have compiled Gaia photometry (DR2) of our sample of M and L dwarfs. The absolute magnitude was estimated using Gaia parallaxes, reddening map for the interstellar extinction (Schlafly & Finkbeiner, 2011), and extinction coefficients for the Gaia photometric system (Casagrande & VandenBerg, 2018). The Gaia database provides no valid parallax measurement for one star from our sample, 2MASS J03184214+0828002, thus the distance measured for its candidate companion (Luhman et al., 2012) was used for the calculations.

As it is shown in Figure 2, the obtained color-magnitude diagram follows a trend in accordance with the expectations based on the Hertzsprung-Russel diagram. It can also be observed, that the different spectral classes occupy different slices on this diagram, although the applied classification was rather limited given the small amount of incorporated spectral templates in `pyhammer`. Our results proved that only a limited spectral classification can be done based on the Gaia photometry alone and it should be complemented by spectroscopy.

5. Summary

A spectral classification was carried out for 20 targets: 16 poorly studied M dwarfs, 3 L dwarfs and one K giant star. Hα emission was detected in 6 objects

(33% of the sample) with evidence of Hα variability in one object. We have compared our spectral classification to Gaia photometry (DR2) concluding that spectral observations are needed for reliable spectral type determination.

Acknowledgements. The authors would like to acknowledge support from ERASMUS+ grant number 2017-1-CZ01-KA203-035562, and the European Union's Horizon 2020 research and innovation programme under grant agreement No 730890 (OPTICON).

References

Casagrande, L. & VandenBerg, D. A., On the use of Gaia magnitudes and new tables of bolometric corrections. 2018, *Mon. Not. R. Astron. Soc.*, **479**, L102, DOI: 10.1093/mnrasl/sly104

Cram, L. E. & Mullan, D. J., Model chromospheres of flare stars.I. Balmer-line profiles. 1979, *Astrophys. J.*, **234**, 579, DOI: 10.1086/157532

Delfosse, X., Forveille, T., Perrier, C., & Mayor, M., Rotation and chromospheric activity in field M dwarfs. 1998, *Astron. Astrophys.*, **331**, 581

Henry, T. J., Ianna, P. A., Kirkpatrick, J. D., & Jahreiss, H., The solar neighborhood IV: discovery of the twentieth nearest star. 1997, *Astron. J.*, **114**, 388, DOI: 10.1086/118482

Kesseli, A., West, A. A., Harrison, B., Veyette, M., & Feldman, D., PyHammer: An Automatic and Visual Suite for Spectral Typing Stars. 2017, in American Astronomical Society Meeting Abstracts, Vol. **229**, *American Astronomical Society Meeting Abstracts #229*, 240.35

Luhman, K. L., Loutrel, N. P., McCurdy, N. S., et al., New M, L, and T Dwarf Companions to Nearby Stars from the Wide-field Infrared Survey Explorer. 2012, *Astrophys. J.*, **760**, 152, DOI: 10.1088/0004-637X/760/2/152

Metodieva, Y., Antonova, A., Golev, V., et al., Low-resolution optical spectra of ultracool dwarfs with OSIRIS/GTC. 2015, *Mon. Not. R. Astron. Soc.*, **446**, 3878, DOI: 10.1093/mnras/stu2370

Mohanty, S. & Basri, G., Rotation and Activity in Mid-M to L Field Dwarfs. 2003, *Astrophys. J.*, **583**, 451, DOI: 10.1086/345097

Reiners, A. & Basri, G., On the magnetic topology of partially and fully convective stars. 2009, *Astron. Astrophys.*, **496**, 787, DOI: 10.1051/0004-6361:200811450

Schlafly, E. F. & Finkbeiner, D. P., Measuring Reddening with Sloan Digital Sky Survey Stellar Spectra and Recalibrating SFD. 2011, *Astrophys. J.*, **737**, 103, DOI: 10.1088/0004-637X/737/2/103

Schöfer, P., Jeffers, S. V., Reiners, A., et al., The CARMENES search for exoplanets around M dwarfs. Activity indicators at visible and near-infrared wavelengths. 2019, *Astron. Astrophys.*, **623**, A44, DOI: 10.1051/0004-6361/201834114

Tody, D., The IRAF Data Reduction and Analysis System. 1986, in Proc. SPIE, Vol. **627**, *Instrumentation in astronomy VI*, ed. D. L. Crawford, 733

Contrib. Astron. Obs. Skalnaté Pleso **49**, 551 – 555, (2019)

Transit modeling of WASP-43b

M.C. Maimone[1,2], F. Tinaut-Ruano[1,3], T. Różański[4] and H. Parviainen[1]

[1] *Instituto de Astrofísica de Canarias*

[2] *Università degli Studi di Torino*

[3] *Universidad de La Laguna*

[4] *University of Wrocław, Astronomical Institute, Kopernika 11, Wrocław, PL-51-622, Poland*

Received: August 12, 2019; Accepted: October 29, 2019

Abstract. The goal of this project was to learn how to estimate basic properties of a transiting exoplanet from ground-based transit photometry. We analysed a photometric time series of a single WASP-43b transit. Data reduction was carried out using a custom-built aperture photometry pipeline written in Python, while a custom light-curve modelling code based on `PyTransit` was used for parameter estimation. We obtained a transit time centre $T_0 = 2\,458\,168.0862 \pm 0.0001$, a radius ratio $R_p/R_\star = 0.121 \pm 0.004$ and an impact parameter $b = 0.71 \pm 0.06$. We compared our results with literature and found agreement within 3σ for almost parameters. The two exceptions were the time of the transit centre, T_0, and the radius ratio, both with significant discrepancy. We believe the T_0 discrepancy is due to the bad accuracy of the period and/or T_0 values, while the radius ratio discrepancy could be due to systematics that were not accounted sufficiently by the linear baseline model used in the transit modelling.

Key words: Extrasolar planets – photometry – exoplanet transits – Bayesian statistics

1. Introduction

Since the discovery of the first planet orbiting a solar-like star (Mayor & Queloz, 1995), the study of exoplanets has become one of the most dynamic research fields in astronomy. With the number of exoplanet detections dramatically increasing in recent years, the field is moving from simple detection and statistical studies to the characterization of individual planets.

The transit method is one of the most powerful means to detect exoplanets and it is based on transits caused by the periodic passage of a planet in front of its host star. Modelling transits provide us with a wealth of precious information on the planet, as explained by Winn (2010).

In this paper we describe our analysis step by step: from the reduction of raw data and the normalisation of stellar light curve (**Data**) to the proper analysis and Bayesian statistics (**Transit Fitting**), it will be possible to understand how we extracted transit parameters of WASP-43b (**Conclusions**).

1.1. WASP-43

The set of data belongs to WASP-43, a star located in the Sextans constellation at 80 pc from the Earth. It is a K7V-type star with V=11 as apparent magnitude in GRP GAIA filter and it hosts a hot Jupiter companion (WASP-43b) far 0.01 AU, with a period of 0.8 days (Hellier et al., 2011). The high brightness, the low level of stellar activity and no presence of other planets made this target perfect to learn the basics of transit analysis.

2. Data

Our dataset was collected on the 18th February, 2018. Observations lasted almost 3 hours and images were acquired with MuSCAT2, an imaging instrument installed in Carlos Sánchez Telescope (TCS) at Teide Observatory, Tenerife, Spain. The sensor covers 0.435" per pixel with a total FoV of 7.43 x 7.43 arcmins. It is equipped with a *griz* filter set (4 filters in total). Only the g filter was used for WASP-43 observations, more than 90% of transmission between 410 and 520 nanometers (IAC, 2019). The dataset consisted of 393 FITS images observed in *g'* passband, 328 of them were time-frames of the target, 50 flat-field frames and 15 bias frames. In order to obtain the light curve and extract planet parameters, it was necessary to carry out a reduction of the raw data because of non-uniform illumination and pixel-to-pixel sensitivity variations. We removed these effects in each time-frame by subtracting the Master Bias[1] and dividing by the Master Flat[2] (previously normalised to one).

2.1. Aperture photometry and differential photometry

The aim of the first part of our project was to obtain a light curve from photometric observations. In order to sum up the star's flux and correct it for background contribution, we made aperture photometry. We selected 2 companion stars similar in brightness and shape to our target, as shown in Figure 1. The similar shape allowed us to take the same aperture radius and annulus radius for all of them ($R_{\mathrm{ap}} = 10$ pixels, $R_{\mathrm{an}} = 20$ pixels) using the Python package `photutils`. *Companion 1* is an early G-type star (V=14 mag), while *companion 2* is a late F-type (V=11 mag). They were observed both by GAIA and magnitudes were measured with the GRP GAIA filter. In order to remove light contamination, we subtracted the background (F_{an}) from stellar fluxes (F_{ap}) in each time-frame. Afterwards, we removed atmospheric systematics and improved the signal-to-noise ratio by performing differential photometry (Winn, 2010), we normalised the flux of our target using the mean of the flux of *companion 1* and *companion 2*. The obtained light curve showed only one transit as reported in Figure 2, where the model is overlapped.

[1]The median of bias frames.

[2]The median of flat-field frames.

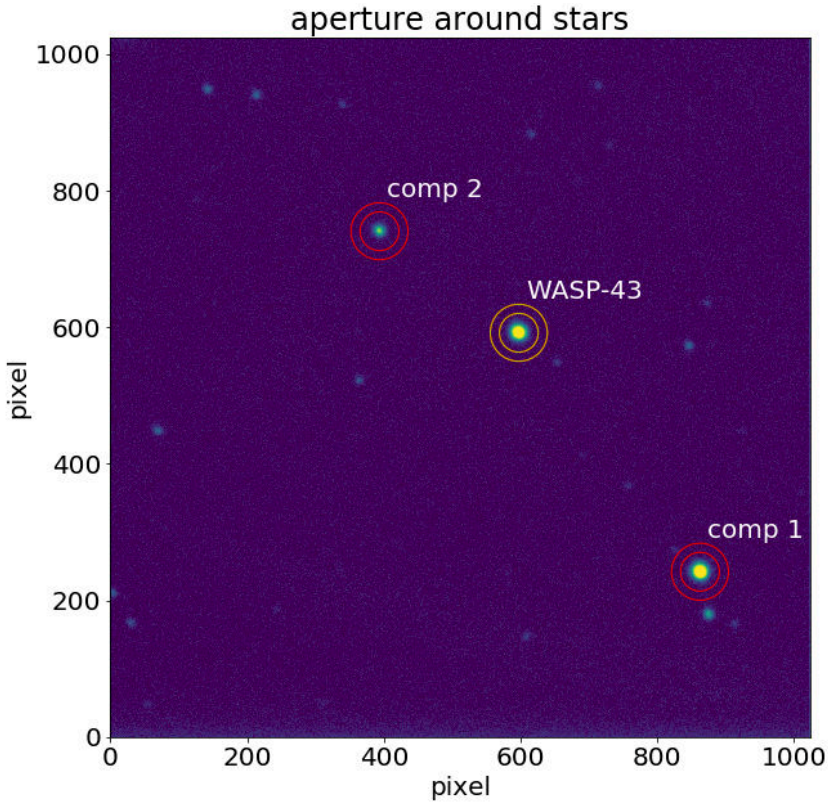

Figure 1. *FoV of WASP-43.* Two stars (companion 1 and 2) were selected to carry out aperture and differential photometry. We chose an aperture radius equal to $R_{ap} = 10$ pixels and an annulus radius equal to $R_{an} = 20$ pixels.

3. Transit fitting

In the second part of the project, we extracted stellar and planetary parameters exploiting Bayesian analysis implemented by the Python software routine `PyTransit` (Parviainen, 2015). A detailed treatment of Bayesian methods could be find in Parviainen (2018). We fitted 8 parameters: baseline slope and intercept, limb darkening coefficients, stellar density, impact parameter, radius ratio and period[3]. We carried out a preliminary analysis using Differential Evolution Algorithm (DEA) in order to obtain an initial set of parameters. They were used as priors for the subsequent MCMC-running in order to get reason-

[3]Our dataset showed only one transit which does not allow to estimate the period. We put an informative prior ($P = 0.81347753 \pm 0.00000071$) on it using a literature value only because it was a requirement of the fitting routine.

able posterior distributions. We used 30 chains of 500 iterations to sample the posterior probability distribution. Results are summarised in Table 1.

Table 1. WASP-43b transit analysis results. [*Comment*: parameterisation in sampling space follows Kipping (2013), where the quadratic limb darkening coefficients u and v are mapped from sampling parameters q_1 and q_1. Notation $\mathcal{U}(a,b)$ denotes uniform distribution over interval $[a,b]$, while $\mathcal{N}(\mu,\sigma)$ normal distribution with mean equals μ, and standard deviation σ].

Name	Unit	Prior	Obtained value	Literature value
Transit centre time	MJD	$\mathcal{N}(0,0.1)$	2458168.0862 $\pm$0.0001	2458168.6029 $\pm$0.0030
Stellar density	g cm^{-3}	$\mathcal{U}(0.1,25)$	2.5 ± 0.4	2.410 ± 0.079
Radius ratio		$\mathcal{U}(0.05,0.25)$	0.121 ± 0.004	0.1595 ± 0.0008
Impact parameter		$\mathcal{U}(0,1)$	0.71 ± 0.06	0.656 ± 0.010
Limb darkening u		see comment	1.0 ± 0.3	0.983 ± 0.050
Limb darkening v		see comment	-0.2 ± 0.3	0.065 ± 0.060
Nuisance parameters				
Error logarithm		$\mathcal{U}(-4,0)$	-3.041 ± 0.017	
Baseline slope s		$\mathcal{N}(0,0.1)$	-0.0095 ± 0.0015	
Baseline intercept		$\mathcal{N}(1,0.1)$	1.0010 ± 0.0001	

Results show that almost all parameters are compatible within 3σ with the literature values (Gillon, M. et al., 2012), except for the T_0 and the radius ratio. The discrepancy between values of T_0 could be ascribable both to a bad accuracy of the period and/or T_0. A full O-C analysis could confirm our hypothesis, but unfortunately it was out of scope of the project.

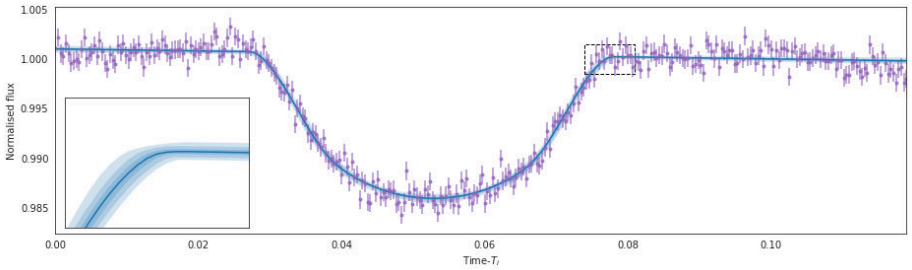

Figure 2. Transit of WASP-43b, centred to T_0. Data coming from Carlos Sánchez Telescope are shown in purple, while the best fit model in blue. The lower right-hand corner shows the zoomed part with median-centred 68%, 95%, and 99.7% central posterior intervals. T_i is the initial time point in our sequence in BJD (2458168.033).

4. Conclusions

The goal of the project was to learn how to estimate exoplanet transit parameters from ground-based photometric observations. We analysed WASP-43b dataset. After removing instrumental effects, we carried out aperture photometry and differential photometry in order to sum up the light of selected stars, subtract the background flux and obtain the stellar light-curve. We subsequently extracted the main planet parameters by exploiting Bayesian analysis and MCMC simulations implemented in `PyTransit`. We obtained results shown in Table 1. We compared our results with those present in literature and we found a good match ($< 3\sigma$) for almost all parameters, while there was a significant discrepancy for T_0 and radius ratio (more than 5σ). We believe the T_0 discrepancy is imputable to a bad accuracy in the period and/or in the predicted T_0, while the difference in radius ratio values could be due to strong systematics generated by the linear baseline model fitting. Future perspectives could be to carry out a full O-C analysis and to use non-linear baseline model fitting in order to unveil the causes of T_0 inaccuracy and avoid systematics in radius ratio deduction, respectively.

References

Gillon, M., Triaud, A. H. M. J., Fortney, J. J., et al., The TRAPPIST survey of southern transiting planets - I. Thirty eclipses of the ultra-short period planet WASP-43. 2012, *A&A*, **542**, A4, DOI: 10.1051/0004-6361/201218817

Hellier, C., Anderson, D. R., Collier Cameron, A., et al., WASP-43b: the closest-orbiting hot Jupiter. 2011, *Astron. Astrophys.*, **535**, L7, DOI: 10.1051/0004-6361/201117081

IAC. 2019, MUSCAT2, https://www.iac.es/es/observatorios-de-canarias/telescopios-y-experimentos/muscat2, online; accessed 25-September-2019

Kipping, D. M., Efficient, uninformative sampling of limb darkening coefficients for two-parameter laws. 2013, *Monthly Notices of the Royal Astronomical Society*, **435**, 2152, DOI: 10.1093/mnras/stt1435

Mayor, M. & Queloz, D., A Jupiter-mass companion to a solar-type star. 1995, *Nature*, **378**, 355, DOI: 10.1038/378355a0

Parviainen, H., PYTRANSIT: fast and easy exoplanet transit modelling in PYTHON. 2015, *Mon. Not. R. Astron. Soc.*, **450**, 3233, DOI: 10.1093/mnras/stv894

Parviainen, H. 2018, *Bayesian Methods for Exoplanet Science*, 149

Winn, J. N., Transits and Occultations. 2010, *arXiv e-prints*, arXiv:1001.2010

Contrib. Astron. Obs. Skalnaté Pleso **49**, 556 – 560, (2019)

Application of broadening functions to eclipsing binaries and planetary transits

B. Cseh[1], M. Fedurco[2], R. Komžík[5], P. Mikołajczyk[3], F. Murphy-Glaysher[4], T. Pribulla[5,6] and O. Shubina[7]

[1] *Konkoly Thege Miklós Astronomical Institute, Research Centre for Astronomy and Earth Sciences, Konkoly Thege Miklós út 15-17, H-1121 Budapest, Hungary*

[2] *Institute of Physics, Faculty of Science, P.J. Šafárik University, Park Angelinum 9, 040 01 Košice, Slovakia*

[3] *Astronomical Institute, University of Wrocław, ul. M. Kopernika 11, 51-622 Wrocław, Poland*

[4] *Astrophysics Research Institute, Liverpool John Moores University, 146 Brownlow Hill, Liverpool L3 5RF, U.K.*

[5] *Astronomical Institute of the Slovak Academy of Sciences 059 60 Tatranská Lomnica, The Slovak Republic*

[6] *Gothard Astrophysical Observatory, ELTE, Szent Imre Herceg utca 112, H-9700 Szombathely, Hungary*

[7] *MAO NASU, 27, Akademika Zabolotnoho street, Kyiv, 03680, Ukraine*

Received: August 7, 2019; Accepted: October 7, 2019

Abstract. The broadening-function technique was applied to three binaries and a transiting exoplanet. The faint secondary component in IN Vir was detected. BD And was found to be a triple star. The rotational axis of the primary component of α CrB was found to be practically perpendicular to the orbital plane. A transiting planet signature was clearly found in Kelt-7b data.

Key words: techniques: radial velocities – binaries: eclipsing – planetary systems

1. Introduction

The broadening-function (BF) technique was developed by Rucinski (1992) to analyse close binaries with rotationally broadened spectral lines. The technique uses deconvolution of a target spectrum by a sharp-line template of the same spectral type. The information is extracted from the whole spectrum, as for the cross-correlation function (CCF). Unlike the CCF, BF extraction does not decrease the spectral resolution, allowing the identification of faint companions, planetary transits, non-radial pulsations, starspots etc.

2. Observations and data analysis

New observations were obtained using MUSICOS-clone échelle spectrograph fiber fed from 1.3m Nasmyth-Cassegrain telescope at the Skalnaté Pleso observatory of the Astronomical Institute of the Slovak Academy of Sciences. The CCD frames were first photometrically reduced and cleaned of cosmic rays. Then aperture spectra were extracted, wavelength calibrated, normalized and combined to 1D spectra (for details see Pribulla et al. (2009)).

The 1D spectra were analyzed using a package of routines in IDL. The BFs were extracted from 4900–5400 Å spectral range and 3.5 km s^{-1} radial-velocity (RV) step. The extracted BFs were then smoothed to match the spectral resolution convolving them with the Gaussian function. The RVs were obtained by fitting the Gaussian functions or limb-darkened rotational profiles to BFs as appropriate. The IDL routines were also used to determine heliocentric correction of RV and to compute heliocentric mid-exposure times.

3. Results

3.1. IN Vir

IN Vir ($V = 9.131$, K2III) is a non-eclipsing binary system with orbital period ∼8.22 days. Strassmeier (1997) performed Doppler mapping of the primary component but could not detect the secondary.

BFs of IN Vir were extracted using HD 185144 (K0V) as a template. 27 spectra obtained from March 30, 2017 to June 13, 2019 enabled detection of the secondary component for the first time (see also Volkov et al., 2019). RVs determined from BFs give the following preliminary spectroscopic elements: $V_0 = +40.2 \pm 0.3$ km s^{-1}, $K_1 = 48.9 \pm 0.4$ km s^{-1}, and $K_2 = 69.6 \pm 0.1$ km s^{-1}. It is interesting to note, that on June 13, 2019 a strong flare on the secondary component was observed (see Fig. 1(a)).

3.2. BD And

BD And ($V = 10.84$, F8V) is an eclipsing binary of β Lyr type with period ∼0.926 days. Timing variability indicated an additional component in the system with an orbital period of ∼9 years (Kim et al., 2014).

Forty-four spectra of BD And were obtained from June 3, 2017 to October 8, 2018. BFs were extracted using HD 65583 (G8V) as a template. BFs conclusively confirm the presence of another component in the system revolving on a long-period orbit. The phase-dependence of BFs of BD And showing all three components is in Fig. 1(b). This first spectroscopy of the system promises reliable determination of component parameters and orbital elements.

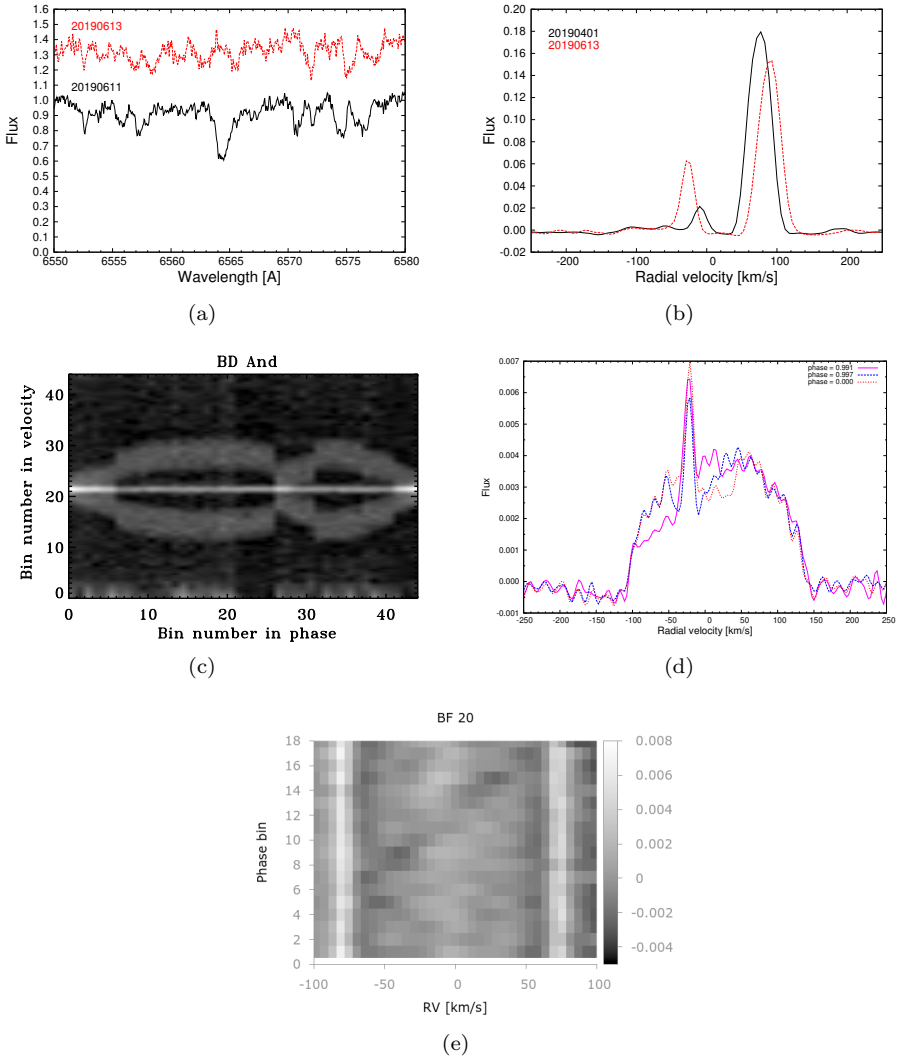

Figure 1. (a) Spectra of IN Vir during the flare (red line) and in quiescence (black line). (b) BFs of IN Vir showing both components and the increase of the BF strength during the flare on the secondary component on June 13, 2019. (c) BFs of BD And ordered in phase showing all three components. (d) Primary eclipse of Alpha CrB visible as a notch progressing from negative to positive radial velocities. The secondary component is the narrow peak on top of the primary component profile. (e) A planet crossing the disk of HD 33643 is seen as a dark streak. Vertical white bands correspond to projected rotational velocity of the parent star.

3.3. α CrB

α CrB (V=2.24, A0V+G5V), is an Algol-type eclipsing binary with period of ∼17.3599 days. The system was recently studied by Schmitt et al. (2016), who determined reliable parameters of components and orbital parameters. Moreover, historical RVs were used to estimate the apsidal-motion period as 6600–10600 yrs. No spectroscopy was, however, obtained in eclipses.

New observations of α CrB were obtained from June 3, 2017 to June 13, 2019. The observations fully cover the primary minimum. The corresponding BF sequence is shown in Fig. 1(c). The progression of the secondary component's shadow is consistent with the spin axis-orbital co-alignment.

3.4. HD 33643

HD 33643 or Kelt-7 (V = 8.54, F2) is a ∼1.5 $M_{\odot}$ star orbited by a planetary-mass companion in ∼2.73 days (Bieryla et al., 2015).

The new observations obtained on October 11, 2018 cover the planetary transit across the disk of the parent star. BFs were extracted using HD 128167 as the template. Fig. 1(d) shows residuals after modelling of BFs by limb-darkened rotational profiles. Detected transit phenomenon is clearly seen and can be modelled in the future. The signal-to-noise ratio of the event could possibly be increased by using a better matching template spectrum.

4. Conclusions

The BF deconvolution technique was found to be a method of choice for the study of binary and multiple systems of stars and exoplanets as well. Unlike CCFs, the extracted BFs can be fitted by complex models (including proximity effects, spots, exoplanet transits, non-radial pulsations or differential rotation). Although the CCF technique is primarily used to measure RVs, the BF technique can outperform it if the components are fast rotators or if faint companions are accompanying the dominant object.

Acknowledgements. The authors would like to acknowledge support from ERASMUS+ grant number 2017-1-CZ01-KA203-035562, and the European Union's Horizon 2020 research and innovation programme under grant agreement No 730890 (OPTICON). BC acknowledges support from the Hungarian National Research, Development and Innovation Office NKFIH Grant KH-130405. FMG acknowledges a PhD Studentship from the UK Science and Technology Facilities Council. PM acknowledges support from Polish National Science Center grant no. 2016/21/B/ST9/01126.

References

Bieryla, A., Collins, K., Beatty, T. G., et al., KELT-7b: A Hot Jupiter Transiting a Bright V = 8.54 Rapidly Rotating F-star. 2015, *Astron. J.*, **150**, 12, DOI: 10.1088/0004-6256/150/1/12

Kim, C.-H., Song, M.-H., Yoon, J.-N., Han, W., & Jeong, M.-J., BD Andromedae: A New Short-period RS CVn Eclipsing Binary Star with a Distant Tertiary Body in a Highly Eccentric Orbit. 2014, *Astrophys. J.*, **788**, 134, DOI: 10.1088/0004-637X/788/2/134

Pribulla, T., Rucinski, S. M., Blake, R. M., et al., Radial Velocity Studies of Close Binary Stars. XV. 2009, *Astron. J.*, **137**, 3655, DOI: 10.1088/0004-6256/137/3/3655

Rucinski, S. M., Spectral-Line Broadening Functions of WUMa-Type Binaries. I. AW UMa. 1992, *Astron. J.*, **104**, 1968, DOI: 10.1086/116372

Schmitt, J. H. M. M., Schröder, K. P., Rauw, G., et al., The α CrB binary system: A new radial velocity curve, apsidal motion, and the alignment of rotation and orbit axes. 2016, *Astron. Astrophys.*, **586**, A104, DOI: 10.1051/0004-6361/201526662

Strassmeier, K. G., Doppler imaging of stellar surface structure. III. The X-ray source HD 116544 = IN Virginis. 1997, *Astron. Astrophys.*, **319**, 535

Volkov, I. M., Kravtsova, A. S., Pribulla, T., et al., Cool spotted binary system IN Vir (HD116544). 2019, *Contributions of the Astronomical Observatory Skalnate Pleso*, **49**, 439

PRÁCE ASTRONOMICKÉHO OBSERVATÓRIA
NA SKALNATOM PLESE
XLIX, číslo 3

Zostavovatelia:	Dr. Petr Kabath
	Dr. Heidi H. Korhonen
	Dr. David Jones
	RNDr. Richard Komžík, CSc.
Vedecký redaktor:	RNDr. Augustín Skopal, DrSc.
Vydal:	Astronomický ústav SAV, Tatranská Lomnica
IČO vydavateľa:	00 166 529
Periodicita:	3-krát ročne
ISSN (on-line verzia):	1336-0337
CODEN:	CAOPF8
Rok vydania:	2019
Počet strán:	74

Contributions of the Astronomical Observatory Skalnaté Pleso are processed using LaTeX 2ε CAOSP DocumentClass file 3.06 ver. 2017.